

Dopaminergic basis for signalling belief updates, but not surprise, and the link to paranoia

Authors

Matthew M Nour^{*1,2,3,4}, Tarik Dahoun^{2,3,5}, Philipp Schwartenbeck^{4,6,7,8,9}, Rick A Adams^{10,11}, Thomas HB FitzGerald^{4,6,12}, Christopher Coello¹³, Matthew B Wall¹³, Raymond J Dolan^{4,6}, Oliver D Howes^{*1,2,3}.

Author Affiliations

1. Institute of Psychiatry, Psychology and Neuroscience (IOPPN), King's College London, London, UK
2. MRC London Institute of Medical Sciences (LMS), London, Hammersmith Hospital, London, UK
3. Institute of Clinical Sciences, Imperial College London, London, UK
4. Max Planck UCL Centre for Computational Psychiatry and Ageing Research, University College London, London, UK
5. Department of Psychiatry, University of Oxford, Oxford, UK
6. Wellcome Trust Centre for Human Neuroimaging (WCHN), University College London, London, UK
7. Oxford Centre for Functional MRI of the Brain (FMRIB), University of Oxford, Oxford, UK
8. Centre for Cognitive Neuroscience, University of Salzburg, Salzburg, Austria
9. Neuroscience Institute, Christian-Doppler-Klinik, Paracelsus Medical University Salzburg, Salzburg, Austria
10. Institute of Cognitive Neuroscience (ICN), University College London, London, UK
11. Division of Psychiatry, University College London, London, UK
12. School of Psychology, University of East Anglia, East Anglia, UK
13. Imanova Centre for Imaging Sciences (Invicro Ltd). Hammersmith Hospital, London, UK

*** Corresponding Authors**

Dr Matthew Nour, matthew.nour@kcl.ac.uk

PO63 Level 5, IOPPN, King's College London, 16 De Crespigny Park, London SE5 8AF

Professor Oliver Howes, oliver.howes@kcl.ac.uk

PO63 Level 5, IOPPN, King's College London, 16 De Crespigny Park, London SE5 8AF

Classification

Biological Sciences / Neuroscience

Social Sciences / Psychological and Cognitive Science

ABSTRACT

Distinguishing between meaningful and meaningless sensory information is fundamental to forming accurate representations of the world. Dopamine is thought to play a central role in processing the meaningful information content of observations, which motivates an agent to update their beliefs about the environment. However, direct evidence for dopamine's role in human belief updating is lacking. We addressed this question in healthy volunteers who performed a model-based functional magnetic resonance imaging (fMRI) task designed to separate the neural processing of meaningful and meaningless sensory information. We modelled participant behaviour using a normative Bayesian observer model, and used the magnitude of the model-derived belief update following an observation to quantify its meaningful information content. We also acquired positron emission tomography (PET) imaging measures of dopamine function in the same subjects. We show that the magnitude of belief updates about task structure (meaningful information), but not pure sensory surprise (meaningless information), are encoded in midbrain and ventral striatum activity. Using PET we show that the neural encoding of meaningful information is negatively related to dopamine-2/3 receptor availability in the midbrain and dexamphetamine-induced dopamine release capacity in the striatum. Trial-by-trial analysis of task performance indicated that subclinical paranoid ideation is negatively related to behavioural sensitivity to observations carrying meaningful information about the task structure. The findings provide direct evidence implicating dopamine in model-based belief updating in humans, and have implications for understating the pathophysiology of psychotic disorders where dopamine function is disrupted.

Keywords: Bayesian surprise, information-theoretic surprise, aberrant salience, schizophrenia, Kullback-Leibler divergence

SIGNIFICANCE STATEMENT

To survive in changing environments animals must use sensory information to form accurate representations of the world. Surprising sensory information might signal that our current beliefs about the world are inaccurate, motivating a belief update. Here, we investigate the neuroanatomical and neurochemical mechanisms underlying the brain's ability to update beliefs following informative sensory cues. Using multimodal brain imaging in healthy human participants, we demonstrate that dopamine is strongly related to neural signals encoding belief updates, and that belief updating itself is closely related to the expression of individual differences in paranoid ideation. Our results shed new light on the role of dopamine in making inferences, and are relevant for understanding psychotic disorders such as schizophrenia, where dopamine function is disrupted.

INTRODUCTION

In order to successfully navigate the world we need to exploit sensory information to make inferences about the environment.¹ For example, before crossing the road it is sensible to check the traffic lights at a pedestrian crossing to decide whether it is safe to cross or not, drawing on our cognitive model of what traffic lights (the observable information) tell us about the traffic flow (the partially observable, or hidden, environmental state). When the light changes from the ‘red man’ to the ‘green man’ this should cause us to update our belief about the state of the environment to infer it is now safe to cross. Importantly, however, it is also critical to assess the informativeness of any sensory input. For example, although it would be surprising to see both the green and red lights on simultaneously, it is not advisable to update one's beliefs about traffic flow based on this observation alone. Thus, adaptive behaviour depends on an ability to discriminate between observations carrying relevant information for the task at hand (informative or *meaningful* cues) and observations carrying irrelevant, ambiguous or no information (non-informative or *meaningless* cues). The former should induce updates in an agent's model of the world, whereas the latter should not.²

Dopamine may play a key role in the processing of meaningful sensory information. Phasic activity in midbrain dopamine neurons is implicated in processing unexpected and salient environmental stimuli,³ including those that are novel⁴⁻⁶ and associated with reward.^{7,8} More recent evidence suggests a role for dopamine in updating a rich internal model of the task environment, necessary for flexible behaviour.⁹⁻¹¹ Specifically, phasic midbrain dopamine signals can reflect inferences about the identity of hidden task states^{12,13} and encode value-neutral prediction errors,^{14,15} as well as support stimulus-stimulus associative learning.¹⁰ Here, we test whether dopamine is associated with the processing of meaningful sensory information in humans, so as to allow an agent to make inferences on a sensory input and appropriately update their internal representations of the environment.

Meaningful information can be formally quantified as the degree to which a new observation changes an agent's prior belief about the current state of the world, given previous observations, to a new (posterior) belief. The magnitude of this belief update from a ‘prior’ belief to a ‘posterior’ belief is usually quantified as the Kullback-Leibler divergence (D_{KL}), and has been termed ‘Bayesian surprise’ (**SI Appendix Eq. 8**).^{2,16}

Belief updates occur after unexpected observations, but unexpectedness alone should be insufficient to motivate change in an agent's internal representations. As outlined in our example above, unexpected observations that are equally unlikely under all competing hypotheses about the

environment contain no meaningful information with respect to the hidden state. The improbability of an observation, given an agent's prior expectation, is often quantified in terms of information-theoretic surprise (I_s , or 'surprisal'), which can be thought of as 'counter evidence' to an agent's representation of the world (**SI Appendix Eq. 9**).

The distinction between the pure unexpectedness (information-theoretic surprise) of an observation and its meaningful information content (Bayesian surprise) is central to understanding how new information influences adaptive behaviour, and may also be of relevance for understanding psychotic symptoms in schizophrenia. One theoretical formulation postulates that stimulus-locked dopamine neural activity is important for processing salient stimuli, and that maladaptive dopaminergic activity in response to ambiguous, unreliable or behaviourally irrelevant (meaningless) events leads to aberrant attribution of salience to these same events. This in turn is thought to underpin mis-attribitional symptoms such as paranoia.^{17–23} Of note, the detection of behaviourally salient stimuli involves a number of brain circuits that modulate the firing of dopamine neurons in the midbrain. In particular, the anterior hippocampus has a key role in regulating midbrain dopamine neuron activity depending on the novelty and context of stimuli via a circuit that involves the nucleus accumbens and ventral pallidum.^{5,20,24}

An understanding of the mechanisms underlying belief updating is therefore critical for understanding both the generation of complex goal-directed behaviours, and symptoms of certain neuropsychiatric disorders. Recent functional magnetic resonance imaging (fMRI) studies have begun to investigate the neural correlates of belief updating in humans, showing that encoding of *unsigned* belief updates (but not simple unexpectedness) is present in dopamine-rich midbrain regions, specifically the ventral tegmental area (VTA) and substantia nigra (SN).^{25–27} However, to date, there is no evidence linking direct measures of dopamine function to belief updating in humans.

We investigated a dopaminergic basis for belief updating using a model-based fMRI-task, combined with PET imaging of dopamine function. We used a task that separates Bayesian surprise, information-theoretic surprise, and reward prediction errors, on a trial-by-trial basis (**Fig. 1**).²⁷ In brief, during the task participants ($n=39$) need to track which of two (hidden) task states pertained at every trial, based on imperfectly informative observations about state identity. Specifically, they were tasked to infer whether visual or auditory cues were currently relevant for predicting monetary outcomes, where the relevant modality signalled the sign of the monetary outcome with approximately 90% cue validity. The identity of the relevant modality reversed (switched) periodically. Participants were not explicitly

informed of the validity of the relevant cue or the reversal probability, but were thoroughly trained on the task prior to scanning.

At the start of each trial, two cues (one auditory, one visual) were presented simultaneously, and could either be incongruent or congruent in their monetary predictions. Following cue presentation participants observed a monetary outcome (either a win or a loss), and subsequently indicated their belief about the relevant predictive modality (current environmental state) on a rating bar (see **Fig. 1**). Monetary outcomes that were unexpected under a current prior hypothesis (rendering $I_s > 0$) could provide either meaningful ($D_{KL} > 0$, in incongruent trials) or meaningless ($D_{KL} = 0$, in congruent trials) information regarding the identity of the task-relevant modality. This design allows a decorrelation of Bayesian (D_{KL}) and information-theoretic (I_s) surprise,^{27,28} enabling us to identify the neural signature of each construct. We hypothesized that belief updates (correlating with the meaningful information content of an observation), but not sensory unexpectedness, would be encoded in dopamine-rich brain areas, namely the SN/VTA complex and ventral striatum, in line with predictions from previous findings.²⁵⁻²⁷ Moreover, we tested whether deviations from optimal behaviour in this task were related to the presence of subclinical paranoid thoughts, a key prediction of the aberrant salience hypothesis of schizophrenia.

To test directly the role of dopamine in these processes, we used positron emission tomography (PET) with the dopamine-2/3 receptor (D2/3R) agonist ligand [¹¹C]-(+)-4-propyl-9-hydroxy-naphthoxazine ([¹¹C]-(+)-PHNO) at baseline (n=36) and following 0.5mg/kg dexamphetamine challenge (n=17). The baseline [¹¹C]-(+)-PHNO PET scan measures D2/3 autoreceptor availability in the midbrain, which are inhibitory receptors.²⁹⁻³¹ We hypothesised that greater midbrain D2/3R availability, reflecting greater tonic inhibitory tone, would be negatively related to phasic midbrain neural response during belief updates.⁴ Following acute amphetamine challenge there is an increase in dopamine concentration in the striatum, consequent upon blockade of dopamine re-uptake,^{4,32} and also possibly due to increased dopamine neuron firing.³³⁻³⁵ Greater dexamphetamine-induced dopamine release is thought to be associated with more spontaneous dopamine transients in the drug-free state, indicating a lower signal-to-noise ratio in dopaminergic signaling.¹⁷ Consequently, we hypothesized that greater striatal dopamine release capacity would be associated with lower ventral striatal neural response during belief updates. Finally, by measuring the D2/3R availability in the striatum at baseline, we were able to test an hypothesised inverted-U relationship between cognitive flexibility and striatal dopamine function at rest.³⁶

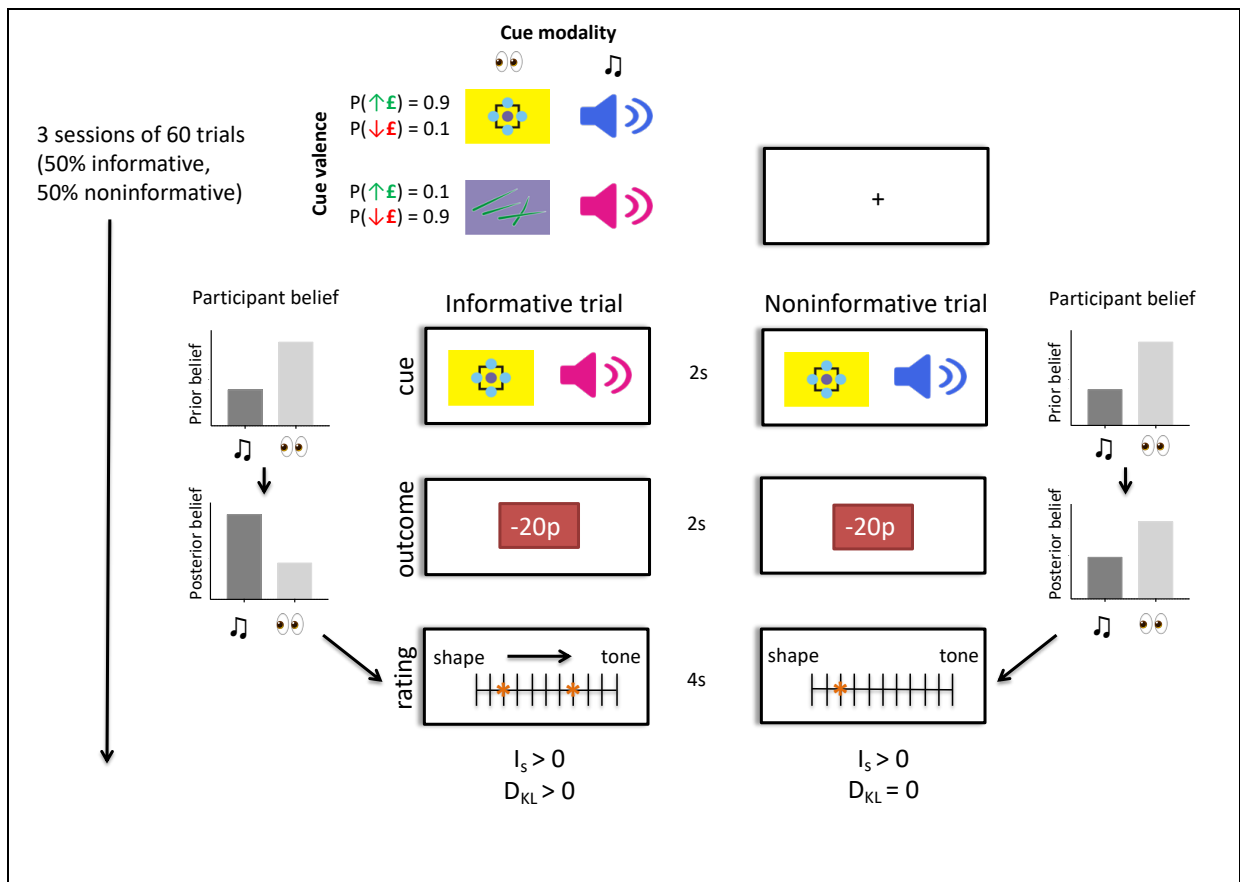


FIGURE 1

fMRI task showing two example trials, one informative and one noninformative. The task contained two auditory and two visual cues, with one cue from each modality being predictive of a monetary win and the other of a monetary loss (approx. 90% validity). Trials started with the simultaneous presentation of one visual and one auditory cue, followed by a monetary outcome (gains or losses from 10-30p). For any given trial only one cue modality was relevant for predicting the outcome, and the identity of the relevant cue switched 5-6 times in a session of 60 trials. The goal of the task was to correctly track the identity of the relevant cue modality (i.e. the hidden task state) at each trial, using information from cue-outcome observations. At the end of each trial participants reported their belief about the identity of the relevant modality using a rating scale. Half of the trials were noninformative, in that the visual and auditory cues predicted the same (congruent) monetary outcome, whilst the other half were informative, in that auditory and visual cues predicted incongruent outcomes. Unexpected outcomes in both informative and noninformative trials had positive information-theoretic surprise (I_s), but these events were only associated with positive Bayesian surprise (D_{KL}) in informative trials.

RESULTS

Task behaviour, computational modelling and relationship to baseline striatal dopamine function

We modelled individual participants' behaviour (belief ratings) by fitting a Bayesian observer model, with two free parameters reflecting participants' expectations about the cue validity (ψ) and the probability of state transitions (reversals) at any given trial ($1 - \delta$) (**Fig. 2**). Together, these parameters captured individual differences in trial-by-trial belief updating. Specifically, the magnitude of a belief update following an unexpected and informative observation is proportional to participants' expectations about cue validity (ψ), whilst their estimate of the state transition probability on a given trial ($1 - \delta$) governs belief uncertainty with each time step. This computational model allowed us to quantify trial-by-trial belief updates as the Kullback-Leibler divergence from 'prior' beliefs to 'posterior' beliefs (**SI Appendix Eq. 8**) (Bayesian surprise), as well as the information-theoretic surprise (surprisal) of an observation (**SI Appendix Eq. 9**) at the monetary outcome stage of each trial.

Our fitted model had high accuracy in explaining participants' behaviour ($R^2 = .67$, 95% confidence intervals = [.60, .73]). Moreover, we found a strong positive correlation between participants' ratings and those predicted by an ideal Bayesian observer model (an instantiation of our computational model using the true parameters of the task) ($r = .75$, [.69, .80]), supporting the idea that participants performed the task adequately, and that their behaviour was closely approximated by a simple Bayesian observer model (**Fig. 3a**). There was no significant correlation between the two free parameter estimates (averaged over task blocks) within participants ($r = .07$ [-.25, .38], $P = 0.65$. Mean [SD] for ψ and δ were 0.90 [0.09] and 0.92 [0.08], respectively), indicating that each captured different aspects of task performance (see **SI Appendix Table S1** for individual participant parameter estimates).

We analysed both overall behavioural performance and trial-by-trial belief updating. We operationalized overall performance as the correlation between participant belief ratings and those of an ideal Bayesian observer (i.e. approximation to normative Bayesian behaviour), whilst our primary measure of trial-by-trial behaviour was the mean difference in reported belief update on informative vs. non-informative trials (i.e. behavioural sensitivity to meaningful information). These measures of behaviour were directly correlated ($\rho = .56$ [.29, .75], $P < 0.001$) (**Fig. 3c**). Closer inspection uncovered that poor overall performance was specifically related to the absolute magnitude of reported belief shifts on non-informative trials ($\rho = -.60$ [-.77, -.34], $P < 0.001$), rather than informative trials ($\rho = -.10$ [-.41, .23], $P = 0.53$). This indicates that participants who showed

poor overall performance had reduced behavioural sensitivity to the meaningful information content of cues, and tended to update their beliefs following non-informative observations.

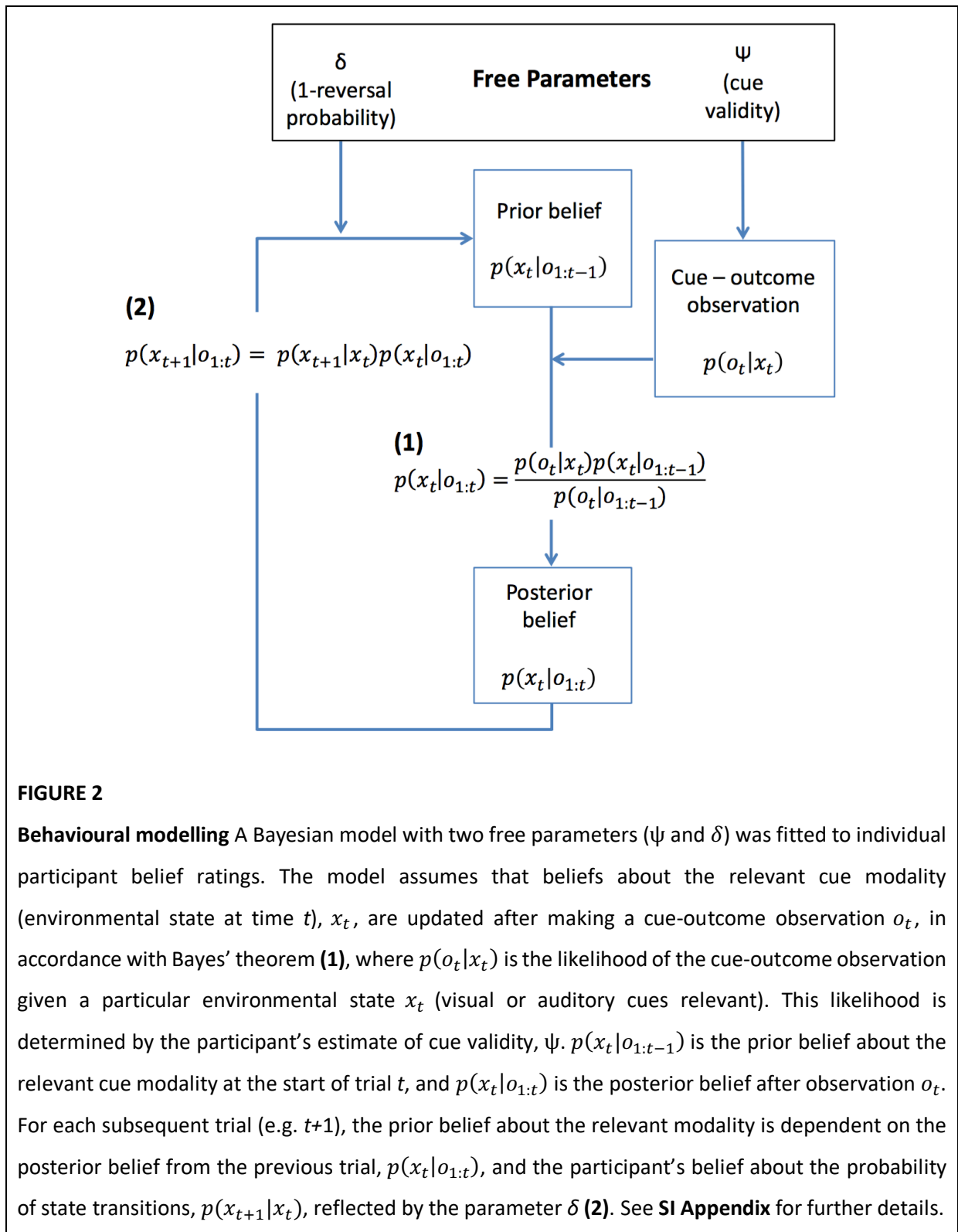


FIGURE 2

Behavioural modelling A Bayesian model with two free parameters (ψ and δ) was fitted to individual participant belief ratings. The model assumes that beliefs about the relevant cue modality (environmental state at time t), x_t , are updated after making a cue-outcome observation o_t , in accordance with Bayes' theorem **(1)**, where $p(o_t|x_t)$ is the likelihood of the cue-outcome observation given a particular environmental state x_t (visual or auditory cues relevant). This likelihood is determined by the participant's estimate of cue validity, ψ . $p(x_t|o_{1:t-1})$ is the prior belief about the relevant cue modality at the start of trial t , and $p(x_t|o_{1:t})$ is the posterior belief after observation o_t . For each subsequent trial (e.g. $t+1$), the prior belief about the relevant modality is dependent on the posterior belief from the previous trial, $p(x_t|o_{1:t})$, and the participant's belief about the probability of state transitions, $p(x_{t+1}|x_t)$, reflected by the parameter δ **(2)**. See **SI Appendix** for further details.

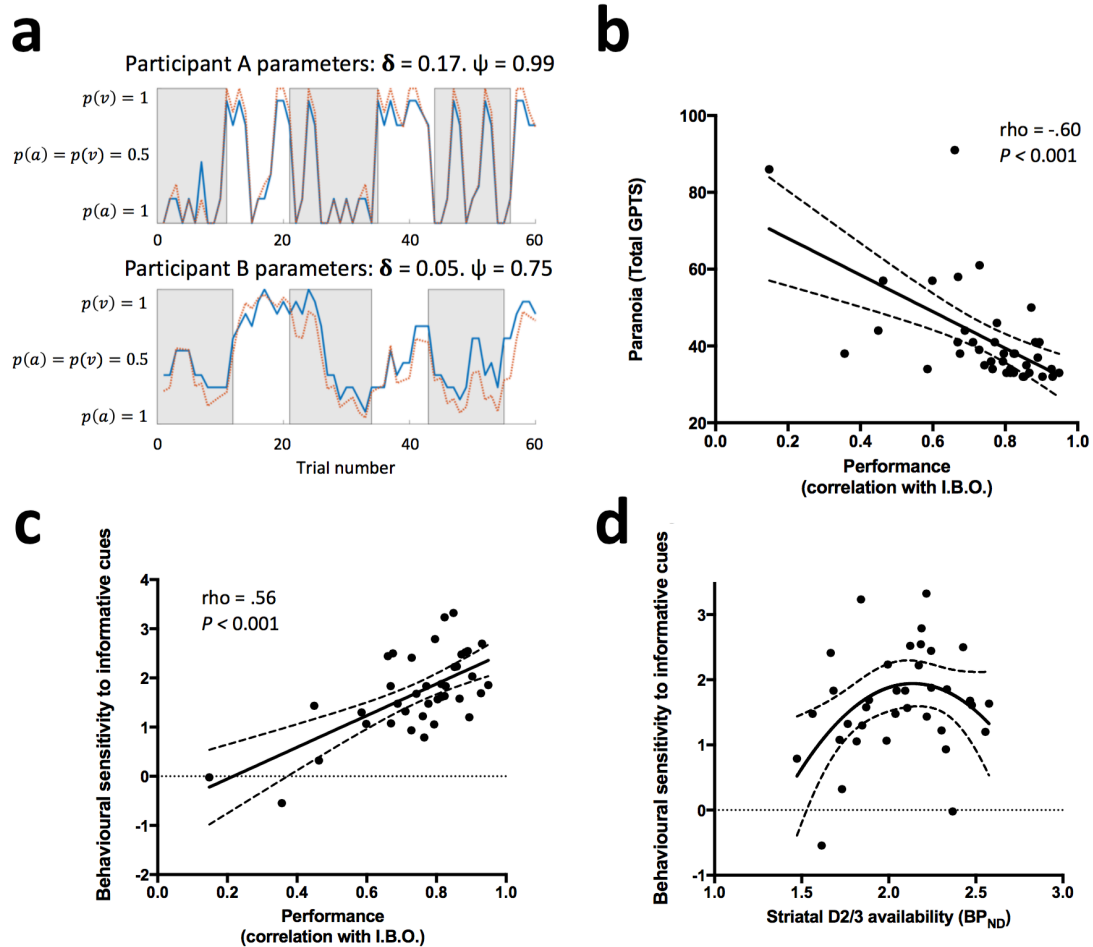


FIGURE 3

Behavioural results (a) Behavioural performance of two exemplar participants in two sessions. Grey/white epochs represent periods when auditory/visual cues are relevant, respectively. The blue solid line displays observed belief ratings at each trial (varying between complete certainty that auditory cues are relevant, $P(a)=1$, and complete certainty that visual cues are relevant, $P(v)=1$). The orange broken line displays predicted behaviour from the fitted model (participant model parameters given above the plots). **(b)** There was a negative relationship between participants' self-reported paranoia scores (measured with the Green Paranoid Thoughts Scale³⁷) and the degree to which their behaviour correlated with the predictions of an ideal Bayesian observer (I.B.O). **(c)** There was a direct correlation between overall behavioural performance (correlation with I.B.O) and behavioural sensitivity to meaningful information (mean difference in belief shift on informative vs. non-informative trials). **(d)** There was an inverted-U relationship between striatal dopamine 2/3 receptor availability and behavioural sensitivity to meaningful information (mean difference in belief shift on informative vs. non-informative trials) (see **SI Appendix Table 2** for parameters of the quadratic model). Broken trendlines **(b-d)** represent 95% confidence bounds.

Interestingly, we found a negative correlation between participants' subclinical paranoia scores (Green Paranoid Thoughts Scale³⁷ total) and both overall behavioural performance ($\rho = -.60$ [-.77, -.34], $P < 0.001$) and the magnitude of belief shifts on informative vs. non-informative trials ($\rho = -.32$ [-.59, <.001], $P = 0.04$) (**Fig. 3b**). In other words, participants with elevated subclinical paranoid thoughts showed reduced behavioural sensitivity to the meaningful information content of observations. Crucially, we found no significant relationship between overall performance and working memory capacity, measured with digit span assessment ($\rho = -.03$ [-.30, .35], $P = 0.85$), indicating that a lower capacity to retain information *per se* does not account for our findings. For additional trial-by-trial behavioural results see **SI Appendix**.

Next, we investigated the relationship between baseline striatal dopamine function and task performance. Previous work has established that there is an inverted-U relationship between resting striatal dopamine levels and cognitive flexibility, thought to be mediated by tonic stimulation of striatal D2/3 receptors.³⁶ Consistent with this hypothesis, we found that baseline D2/3R availability in the whole striatum predicted trial-by-trial sensitivity to meaningful information (mean belief shift on informative vs. non-informative trials) with an inverted quadratic relationship in a simple regression model including linear and quadratic terms for [¹¹C]-(+)-PHNO BP_{ND} (**Model 1**: $F_{2,33} = 3.42$, adjusted $R^2 = .12$, model $P = 0.04$. P -value for linear and negative quadratic term coefficients = 0.26 and 0.04, respectively). As age and body mass index influence striatal baseline [¹¹C]-(+)-PHNO BP_{ND} ,^{38,39} we repeated this analysis including these as covariates in case they were influencing our findings. The inverted quadratic relationship remained significant in this adjusted model (**Model 2**: $F_{4,31} = 3.40$, adjusted $R^2 = .22$, model $P = 0.02$. P -value for [¹¹C]-(+)-PHNO BP_{ND} linear and negative quadratic term coefficients = 0.10 and 0.01, respectively) (**Fig. 3d** and **SI Appendix Table S2**). Importantly, the linear models relating behavioural performance to striatal baseline D2/3R availability (i.e. omitting the quadratic term) were not significant compared to the null model ($P > 0.18$). Furthermore, the simple linear and quadratic regression models describing the two free parameters (ψ and δ) as a function of striatal D2/3R availability were also not significant compared to the null model (all $P > 0.25$).

Belief updates are encoded in the midbrain and ventral striatum

In the region of interest (ROI) fMRI analysis we found effects for model-derived trial-by-trial estimates of Bayesian surprise (meaningful information) in the bilateral substantia nigra / ventral tegmental area (SN/VTA) complex and ventral striatum (**Fig. 4a**), whereas no such effect was evident for information-theoretic surprise (meaningless information), consistent with previous reports.^{26,27} A formal comparison of regions preferentially encoding Bayesian surprise vs. information-theoretic surprise

($D_{KL} > I_s$) showed significantly greater activation for Bayesian surprise in the SN/VTA and ventral striatum bilaterally (significant activation differences at $P_{\text{peak}} < 0.05$, with small volume correction for SN/VTA and ventral striatum ROI, **SI Appendix Fig. S1**). Importantly, neural encoding of Bayesian surprise in the midbrain and ventral striatum (quantified as the principle eigenvariate of the contrast parameter estimates within each region) did not correlate with individual participant model R^2 or the free parameters of the model (all $P > 0.25$), indicating that variation in fMRI parameter estimates in these regions is not driven by differences in model fit.

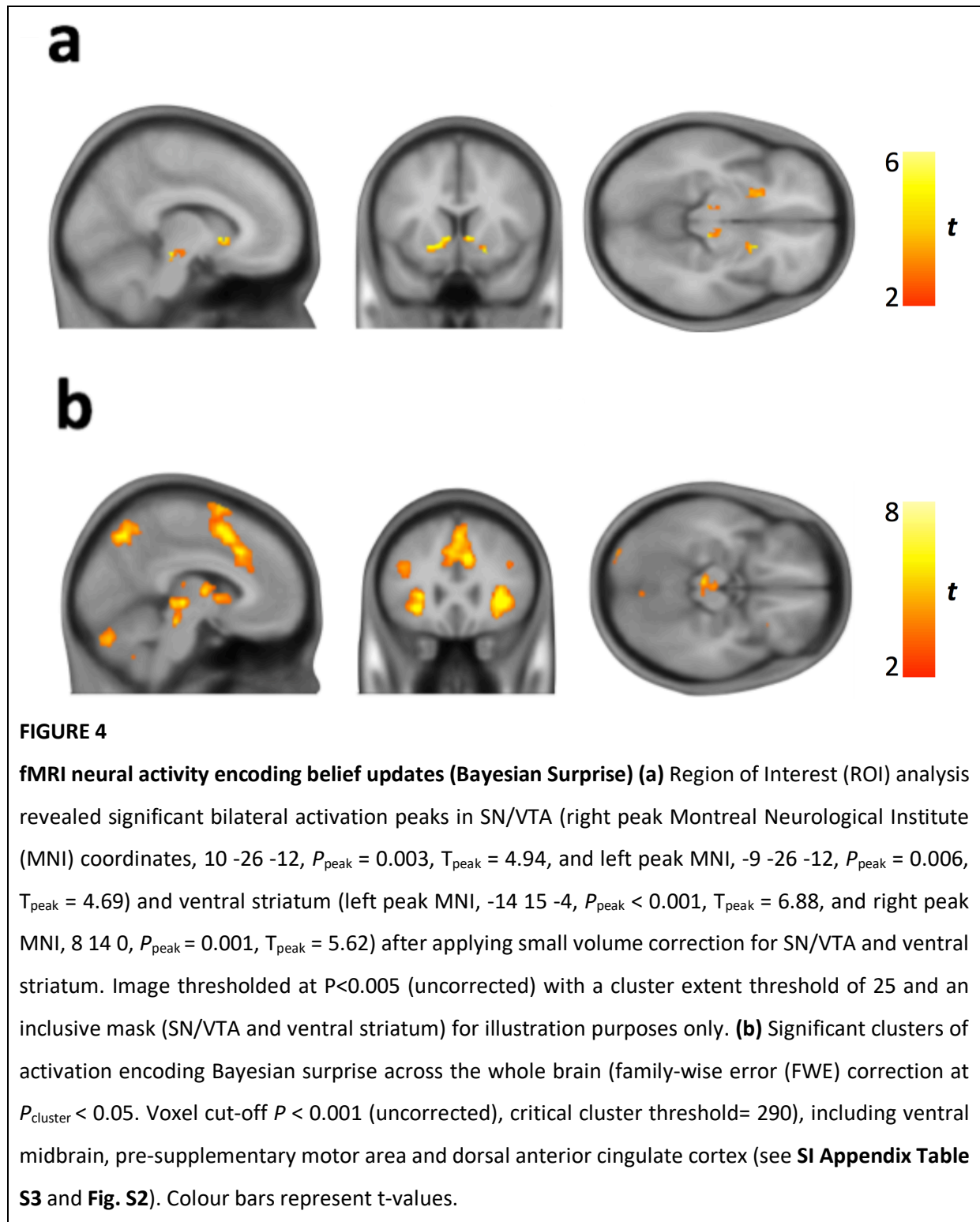
At the whole brain level, we also found effects for Bayesian surprise in the pre-supplementary motor area (pre-SMA), dorsal anterior cingulate cortex, posterior parietal cortex (e.g. supramarginal gyrus) and lateral prefrontal cortex (e.g. middle frontal gyrus) (**Fig. 4b, SI Appendix Fig. S2 and Table S3**). Information-theoretic surprise at monetary outcome was encoded in a network of brain regions including the pre-SMA, anterior insula, middle frontal gyrus, angular gyrus, and precuneus, significant at whole brain $P_{\text{cluster}} < 0.05$ (**SI Appendix Fig. S3a & Table S4**). There was no significant hippocampal activation encoding Bayesian or information-theoretic surprise at monetary outcome, and no activation at cue onset, in a whole brain analysis.

We found no significant correlation between task performance, model parameters or paranoia scores and the effect size of the signal encoding Bayesian surprise in the SN/VTA complex or ventral striatum (all $P > 0.25$), although there was a positive correlation between overall task performance and neural effect size within the pre-SMA encoding information-theoretic surprise ($\rho = .35$ [.03, .61], $P = 0.03$) (**SI Appendix Fig. S3b**).

Beyond neural encoding of Bayesian and information-theoretic surprise, there was no evidence for signed reward prediction error in the SN/VTA complex or the ventral striatum in the ROI analysis, nor at whole brain cluster level at the conventional voxel-level cut-off of $P < 0.001$ (uncorrected). When this cut-off was reduced to a very liberal threshold of $P < 0.05$ (uncorrected), we found a single large cluster involving the left striatum (pallidum, caudate and putamen) significant at whole brain level (**SI Appendix Fig. S4**).

Finally, belief uncertainty at cue presentation (prior uncertainty) was encoded in a widespread network involving dorsolateral prefrontal cortex, medial prefrontal cortex and occipitoparietal cortex. These brain regions were implicated in encoding belief uncertainty both when prior uncertainty was defined from the rating bar report on the previous trial ('subjective uncertainty'), and when it was

defined as the entropy over the distribution of model-derived prior beliefs on the current trial ('model-derived uncertainty', **SI Appendix Eq. 10**) (**SI Appendix Fig. S5** and **Table S5**). The recruitment of a widespread frontoparietal network to encode the uncertainty (entropy) of internal models may reflect the necessity to consider competing hypotheses in working memory.⁴⁰



Dopaminergic basis for neural signals encoding belief updates in midbrain and ventral striatum

Having found evidence consistent with belief update (Bayesian surprise) encoding in midbrain and ventral striatum, we next determined whether this neural encoding was related to *in vivo* measurements of dopamine acquired in the same participants, using [¹¹C]-(+)-PHNO PET. Baseline dopamine-2/3 receptor (D2/3R) availability (measured as the [¹¹C]-(+)-PHNO non-displaceable binding potential, BP_{ND}) was calculated for the SN/VTA complex, where this measure indexes midbrain dopamine autoreceptor availability. In the midbrain, baseline D2/3R availability was negatively related to fMRI-measured neural activation encoding Bayesian surprise ($\rho = -.43 [-.67, -.11]$, $P = 0.009$) (**Fig. 5a**). There was no significant correlation between SN/VTA baseline D2/3R availability and fMRI activation encoding Bayesian surprise within the ventral striatum ($\rho = -.12 [-.44, .23]$, $P = 0.49$).

We next assessed dexamphetamine-induced dopamine release capacity, calculated as the percentage reduction in BP_{ND} from baseline scan to dexamphetamine scan within the whole striatum. This measure is hypothesised to reflect the dopamine system's tendency towards spontaneous transients at rest, which reduces the signal-to-noise ratio of stimulus-locked dopamine bursts.¹⁷ We found a negative correlation between dexamphetamine-induced striatal dopamine release capacity and neural activation within the ventral striatum encoding Bayesian surprise ($\rho = -.71 [-.89, -.34]$, $P = 0.002$) (**Fig. 5b**). This negative relationship was also present when considering dopamine release capacity within the ventral striatum only ($\rho = -.66 [-.87, -.24]$, $P = 0.005$). Dexamphetamine-induced dopamine release capacity in the whole striatum did not correlate with neural activity encoding Bayesian surprise in the SN/VTA ($\rho = -.10 [-.56, .41]$, $P = 0.71$).

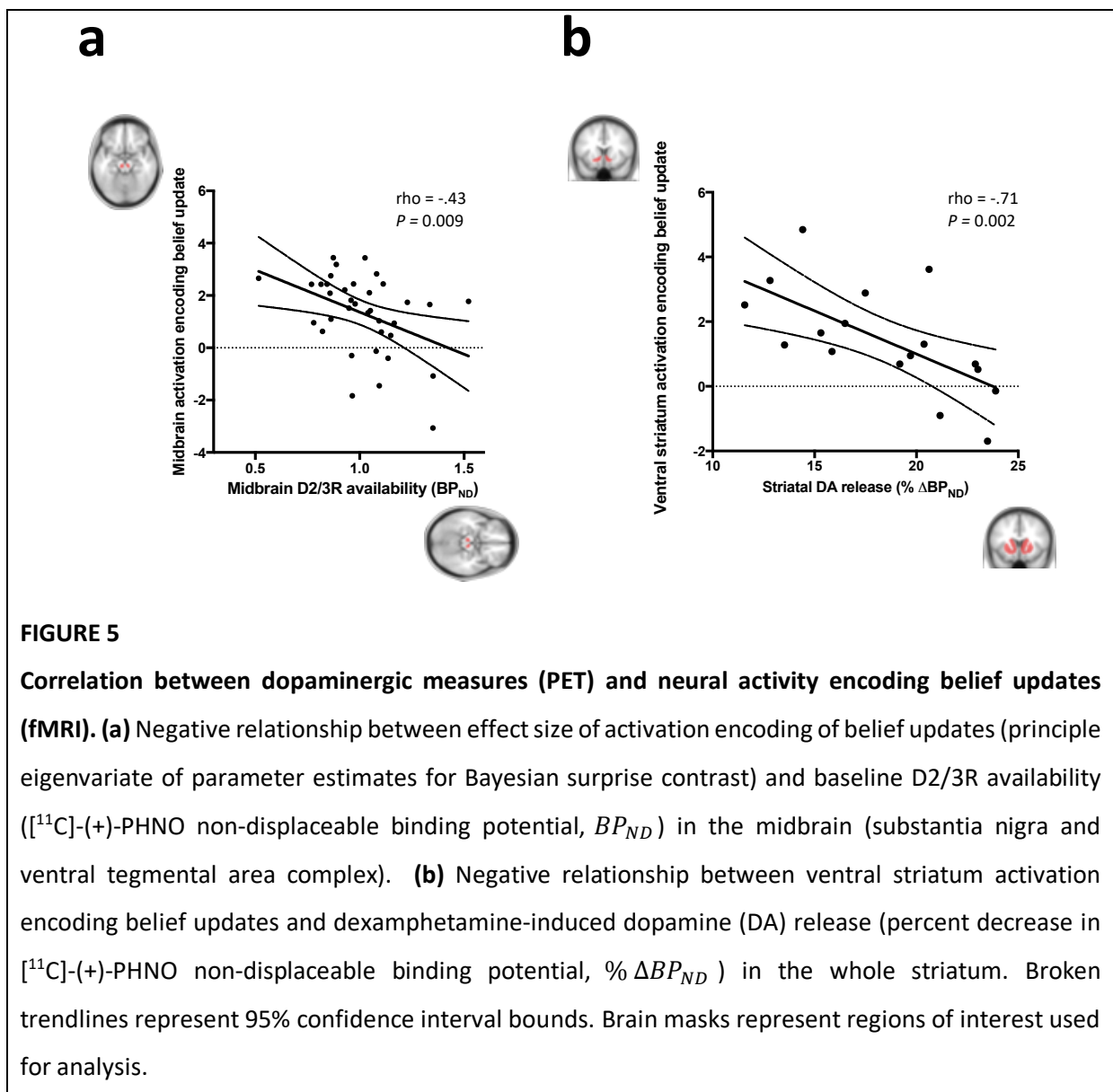
There was no significant relationship between whole striatal D2/3R availability at baseline and either midbrain or ventral striatal fMRI activation encoding Bayesian surprise ($\rho = -.10 [-.43, .24]$, $P = 0.54$ and $\rho = -.05 [-.38, .30]$, $P = 0.79$, respectively).

Testing the specificity of the dopamine-fMRI correlation

Both Bayesian and information-theoretic surprise were encoded in an overlapping medial prefrontal cortex cluster (at whole brain corrected $P_{\text{peak}} < 0.05$, see **Fig. 4b** and **SI Appendix Fig. S3b**), yet there was no significant relationship between the neural activation in the significant voxels for either contrast and midbrain D2/3R availability ($\rho = -.05 [-.38, .30]$, $P = 0.79$ for Bayesian surprise and $\rho = -.27 [-.56, .07]$, $P = 0.11$ for information-theoretic surprise), whole striatal dopamine release capacity ($\rho = .22 [-.31, .64]$, $P = 0.40$ for Bayesian surprise and $\rho = -.45 [-.77, .05]$, $P = 0.07$ for information-

theoretic surprise), or whole striatum D2/3R availability ($\rho = -.06 [-.39, .28]$, $P = 0.73$ for Bayesian surprise and $\rho = .09 [-.25, .42]$, $P = 0.57$ for information-theoretic surprise).

Finally, we conducted four whole brain analyses, testing the negative linear relationship between both midbrain D2/3R availability or whole striatum dopamine release capacity, and neural activation encoding either Bayesian or information-theoretic surprise. These analyses confirmed that neural encoding of Bayesian surprise in the left ventral striatum is negatively correlated with striatal dopamine release capacity (surviving small volume correction at $P_{\text{peak}} < 0.05$, using SN/VTA and ventral striatum ROI, **SI Appendix Fig. S6**). There were no other voxels that showed a significant relationship between neural activation and dopamine measures in any of the four fMRI-PET whole brain analyses, either at whole brain or small volume corrected $P < 0.05$.



DISCUSSION

Controlling for the effects of signed reward prediction errors, we show that the substantia nigra/ventral tegmental area (SN/VTA) and ventral striatum encode meaningful information content in sensory observations. This encoding reflected solely the magnitude of belief updates regarding the current environmental state (Bayesian surprise from prior beliefs to posterior beliefs), but not the simple unexpectedness of an observation (information-theoretic surprise). Using *in vivo* PET imaging of dopamine we also demonstrate that neural activity encoding belief updates is negatively related to dopamine-2/3 receptor (D2/3R) availability in the midbrain, and dopamine release capacity in the striatum. These results provide a direct link between belief updating and dopaminergic function, extending observations from previous fMRI studies that implicate SN/VTA in encoding the magnitude of belief update signals on the one hand,^{25–27} and the assumed role of dopamine in an implementation of probabilistic inference on the other.^{41,42} Additionally, we show that participants' trial-by-trial sensitivity to the meaningful information content of observations has an inverted-U relationship with striatal baseline D2/3R availability, in line with evidence that striatal D2/3R signalling has an inverted-U relationship with cognitive flexibility.³⁶ Our results therefore shed light on the neurochemical basis of belief updating in humans using *in vivo* quantification of dopamine function.

The [¹¹C]-(+)-PHNO signal in the SN/VTA primarily indexes D3 autoreceptor availability^{30,43,44} and the signal here is less sensitive to tonic synaptic dopamine levels compared with the striatum.⁴⁵ D2/3R availability was negatively related to neural activity encoding belief updates in the SN/VTA complex, consistent with evidence that midbrain D3Rs have an inhibitory effect on dopaminergic neurons,^{29,31} and in line with the notion that tonic dopamine signalling may regulate the amplitude of stimulus-locked phasic dopamine neuron activity.⁴ For example, D3R knockout mice have elevated extracellular dopamine levels in the nucleus accumbens,⁴⁶ whilst mice treated with D3R-preferring agonists show reduced dopamine concentration in the accumbens.⁴⁷ In a recent fMRI study, selective antagonism of the D3R enhanced midbrain and ventral striatal fMRI activation during anticipation of monetary reward, providing indirect evidence for an inhibitory role for midbrain D3Rs in humans.⁴⁸ The behavioural significance of elevated midbrain D2/3R availability has also recently been investigated in rats, where nigral [¹¹C]-(+)-PHNO BP_{ND} correlated with impaired reversal learning in a probabilistic reward task.⁴⁹ Our findings extend this work by showing that natural variation in human midbrain D2/3R availability is associated with altered midbrain activation during belief updating, with lower levels associated with relatively greater activation. Moreover, our task design allowed us to investigate the specific role of dopamine in encoding the meaningful information content of an observation, decorrelating this construct from simple unexpectedness and reward prediction error.

We found that a belief update signal in the ventral striatum was negatively correlated with dexamphetamine-induced striatal dopamine release capacity, providing *in vivo* human evidence that this signal is related to dopamine function. This complements findings from a recent optogenetic fMRI study in rats, which demonstrated that striatal BOLD activations may be driven by mesolimbic dopamine neuron firing.⁵⁰ It has been proposed that greater amphetamine-induced dopamine release capacity *in vivo* corresponds to a greater tendency towards spontaneous dopamine neuron firing in the drug-free (baseline) state, which decreases the signal-to-noise ratio of stimulus-locked dopamine bursts.¹⁷ Our finding that striatal dopamine release capacity is negatively correlated with the striatal BOLD response encoding belief updates is therefore consistent with current hypotheses regarding the relationship between amphetamine-induced dopamine release capacity and mesostriatal dopaminergic function at rest. Moreover, this finding extends our understanding by showing a negative relationship between the natural variation in dopamine release capacity in humans, and adaptive neural activation in the ventral striatum. However, it is important to note that the relationship between spontaneous dopamine neuron firing and amphetamine-induced dopamine release has yet to be tested, and that, whilst some studies report that amphetamine's action is dependent on neuronal firing within the VTA,^{33,34} acute amphetamine administration has generally been found to reduce dopamine neuron firing,^{51–53} as well as having other actions to increase striatal dopamine levels.^{4,32,54} Thus, preclinical studies that combine PET and dopamine neuron recordings would be useful to test the hypothesis that spontaneous dopamine neuron firing in the amphetamine-free state is directly associated with dopamine release induced by amphetamine.

Consistent with a previous study using the same task,²⁷ information-theoretic surprise was encoded in frontal brain areas including pre-SMA. We also replicated the finding that the effect size of this activation positively correlated with task performance, suggesting that surprising events may be imbued with higher salience in participants with a better model of the task (resulting in better performance).²⁷ Importantly, there was no relationship between the effect size of the neural response in this region and any PET measure of dopamine function, favouring a more specific role for dopamine in encoding meaningful information.

An influential model proposes that the anterior hippocampus regulates midbrain dopamine neuron firing depending on the novelty and context of stimuli through the descending arm of a hippocampal-VTA loop. Activity in projections from the VTA to the hippocampus, constituting the ascending arm of the loop, in turn facilitate the updating of memory by enhancing long-term potentiation in the

hippocampus.^{5,20} However, we found no evidence for increased hippocampal activity at cue onset, and there was no positive correlation between hippocampal activation and either meaningful (Bayesian) or meaningless (information-theoretic) surprise at monetary outcome. It should be noted, however, that our task was not optimised to detect event-related hippocampal activity relating to novelty processing or learning, as participants had been thoroughly trained on the task stimuli and structure prior to scanning. Nevertheless, further studies are required to investigate the relationship between prediction error signals (e.g. in the midbrain and orbitofrontal cortex) and hippocampal representations, given the proposed role of the hippocampus in the learning and re-mapping of internal models ('cognitive maps').^{11,26,55-57}

It has also been suggested that a connection from the medial prefrontal cortex to the dopaminergic midbrain may convey information relating to inference about the environment (specifically, inference over possible hidden states of a task).¹² In line with this finding we found that belief updates were encoded in the medial frontal cortex, including dorsal anterior cingulate. This observation is consistent with previous human and nonhuman primate studies^{26-28,58,59} as well as with suggestions that anterior cingulate cortex is active in novel or volatile environments wherein agents need to refine their internal models in light of new observations.^{28,60} Moreover, we also detected activation encoding belief updates in lateral prefrontal and posterior parietal cortical regions, which have been implicated in inference on the nature of the causal relationships between observations (hidden causal structures),⁶¹ and in encoding state prediction errors that support learning an internal model of a task (state-action-state transition probabilities).⁶²

The ventral striatum and SN/VTA are implicated in encoding signed reward prediction errors that update action and state values.^{7,63,64} Ventral striatal encoding of these model-free reward prediction errors may be negatively related to ventral striatal dopamine synthesis capacity.^{65,66} Consistent with previous studies using similar task designs,^{27,67} we did not find strong evidence for effects within these regions for signed reward prediction errors. Previous studies have shown that the processing of reward anticipation and prediction error in the mesolimbic dopamine circuit is sensitive to current task demands, including action planning.⁶⁸⁻⁷⁰ In our task participants were not attempting to maximize reward, and the observation of monetary gains vs. losses was not indicative of task performance. Furthermore, unexpected outcomes were equally informative about changes in relevant cue modality, regardless of whether they took the form of a monetary gain or loss. Thus, the important contribution of our results is to highlight dopamine's role in signalling belief updates beyond its role in signalling signed reward prediction errors, an observation that hints at a role for dopamine in probabilistic

inference and structural learning. Consistent with this interpretation, a recent study employing electrophysiological recordings in behaving rats demonstrated that midbrain dopamine neurons that signal classical signed reward prediction errors also signal value-neutral sensory prediction errors.¹⁴ Moreover, in humans the magnitude of value-neutral ‘stimulus identity’ prediction errors in the midbrain is related to updates in state representation in the orbitofrontal cortex.⁷¹ The implication here is that dopamine has a wide range of functions that extends to updating a predictive associative model of the world, suggesting phasic dopamine activity signals a more general error signal, where value-errors are a special case.^{10,14}

The findings of our study are highly relevant for dopaminergic and neurocomputational theories of schizophrenia.^{59,72} The aberrant salience hypothesis proposes that symptoms such as paranoia arise when unwarranted meaning and behavioural salience is attributed to ambiguous, irrelevant or unreliable stimuli.^{17,18,20–23} This is suggested to reflect maladaptive phasic dopamine signalling in a mesostriatal circuit, activity that underpins learning of cue values and associations under normal circumstances.^{7,10,14} Our results speak to this hypothesis in two ways. Firstly, subclinical paranoia was negatively related to behavioural sensitivity to the meaningful information content of an observation, and also to the degree to which a participant’s performance correlated with that of an ideal Bayesian observer. This suggests that maladaptive belief updating (i.e. updating one’s beliefs following ambiguous or meaningless observations) may contribute to the formation of subclinical paranoid beliefs. Secondly, by dissociating the meaningful information content of an observation from its simple unexpectedness, and showing a dopaminergic relationship with the former, our findings point to the possibility of advances that might accrue from reformulating constructs such as ‘salience’ in a more mathematically rigorous fashion. In fact, one hypothesis from our findings is that the central feature of ‘aberrant salience’ in psychotic disorders is a failure to dissociate between meaningful (task-relevant) and meaningless (task-irrelevant) information, resulting in belief updating arising out of merely surprising inputs.⁵⁹

Conclusions

Using model-based fMRI we demonstrate that activity within both the midbrain and ventral striatum correlates with the magnitude of a belief shift following an observation, indicating that these structures encode the meaningful information content of a stimulus, as opposed to its simple unexpectedness (surprise). Moreover, using PET we demonstrate a potential dopaminergic basis for these neural signals. Specifically, neural encoding in the midbrain was negatively related to midbrain D2/3R availability, whilst encoding in the striatum was negatively related to striatal dopamine release

capacity. Finally, we show that participants who displayed the least sensitivity to the meaningful content of observations also reported greater subclinical paranoid ideation. Together, our results suggest that the role of phasic mesolimbic dopamine activity extends beyond its well-established role in signalling signed reward prediction errors, and includes updating a rich internal model of the world capable of supporting flexible behaviour. Furthermore, our findings have relevance for understanding the pathophysiology of psychotic disorders such as schizophrenia, which are characterised by mesostriatal dopamine abnormalities and symptoms arising from aberrant inferences about the world, as manifest in delusions.

MATERIALS AND METHODS

Subjects

The study was approved by the local NHS Research Ethics Committee and the Administration of Radioactive Substances Advisory Committee (ARSAC). Thirty-nine healthy volunteers (17 females, mean age 26.2 yrs [SD 7.0]) were included in the fMRI analysis. Thirty-six subjects also received a baseline [^{11}C]-(+)-4-propyl-9-hydroxy-naphthoxazine ([^{11}C]-(+)-PHNO) scan to quantify dopamine D2/3 receptor (D2/3R) availability in the midbrain. Seventeen subjects additionally received a second [^{11}C]-(+)-PHNO PET scan, timed to start 3hrs after oral administration of dexamphetamine (0.5mg/kg), to quantify dexamphetamine-induced dopamine release in the striatum. See **SI Appendix** for further details.

Task

We used a validated task that de-correlated information-theoretic and Bayesian surprise.²⁷ Subjects performed 3 sessions of the task (60 trials per session) during fMRI after at least 1 hr of training on the task prior to the scan, in which they learned about the task structure and cue valences. For full task details see **Fig. 1** and **SI Appendix**.

Computational modelling

We used a simple Hidden Markov Model that captures trial-by-trial belief updating using iterative application of Bayes' rule (**SI Appendix Eq. 6**).²⁷ The model was fitted to individual subject behaviour by varying two free parameters using constrained maximum likelihood estimation: (1) cue-validity (ψ) and (2) the state transition probability ($1 - \delta$). See **SI Appendix** for further details.

Image acquisition

Structural and functional magnetic resonance (MR) images were acquired using a Siemens MAGNETOM Verio 3-T MR scanner. Functional images were acquired with a multiband sequence based on the multiband EPI WIP v012b provided by the University of Minnesota,^{73–76} using a multiband acceleration factor of 2. We acquired a whole brain volume consisting of 72 interleaved slices (2mm thickness), with a repetition time of 2000 ms, echo time of 30 ms, an in-plane resolution of 3 x 3 mm, flip angle of 62°, and bandwidth of 1906 Hz/pixel. In each task session 402 volumes were acquired (duration = 13 minutes, 24 seconds), totalling 1206 volumes over three task sessions. An MR-compatible button box recorded right index and middle finger presses to move the cursor on the rating bar. Auditory cues were presented using MR-compatible headphones.

Positron emission tomography (PET) images were acquired using a Siemens Biograph HiRez XVI PET scanner. PET acquisition started with the injection of a single intravenous bolus of 0.020-0.029 micrograms/kg [¹¹C]-(+)-PHNO.⁷⁷ For dexamphetamine PET scans 0.5mg/kg dexamphetamine was administered orally 3hrs before [¹¹C]-(+)-PHNO administration, so that scan acquisition coincided with the expected time of peak action.⁷⁸ Across all PET scans the mean [¹¹C]-(+)-PHNO mass administered was 1.5 micrograms (SD 0.31) and mean injected activity was 177.5 MBq (SD 50.0). After the administration of the radiotracer, dynamic emission data were acquired continuously for 90 minutes. For further details of MR and PET image acquisition see **SI Appendix**.

fMRI analysis

fMRI analysis was performed using SPM12 (<http://www.fil.ion.ucl.ac.uk/spm>), and employed standard image preprocessing procedures (outlined in **SI Appendix**). For first-level analysis we used a mass-univariate approach, using a general linear model (GLM) with separate stick function events for the onset of fixation crosses, cues, monetary outcome presentation and rating bars.²⁷ At monetary outcome we included parametric regressors defining: (1) information-theoretic surprise (I_s , z-scored, **SI Appendix Eq. 9**), (2) Bayesian surprise (Kullback-Leibler divergence, D_{KL} , z-scored, **SI Appendix Eq. 8**), (3) the difference between reported belief shifts (derived from observed changes on the rating bar) and estimated shifts in beliefs from the fitted model (z-scored), (4) monetary outcome (+1 for win, -1 for loss), and (5) signed reward prediction errors (observed reward minus expected reward, where expected reward is defined as the sum of the valence of the observed auditory and visual cues, weighted by the prior beliefs about their relevance).

To control for possible confounds we included the following parametric regressors at cue onset: (1) current reported beliefs about relevant modality, (2) subjective uncertainty about these beliefs (derived from the rating bar report on the previous trial), (3) expected relevant outcome value (defined above), and (4) expected irrelevant outcome value (sum of the valence of observed cues weighted by the subject's prior beliefs about their *irrelevance*). We included the number of button presses as a parametric regressor at rating bar onset. Regressors were not serially orthogonalised, to remove shared variance. The GLM described here (GLM1) was used for the main analysis, including the 'subjective uncertainty' fMRI analysis. We defined a second model (GLM2) for the 'model derived uncertainty' fMRI analysis. See **SI Appendix** for further details regarding both GLM1 and GLM2.

A standard summary statistic approach was used to test for second level effects of Bayesian surprise (D_{KL}) and information-theoretic surprise (I_s) at monetary outcome using one-sample t-tests on the estimated responses for the first level analysis, and a t-contrast of $D_{KL} > I_s$ to identify brain regions that showed preferential activation for belief updates compared with sensory unexpectedness. Random field theory was used to correct for multiple comparisons.

Our fMRI analysis focused on an *a priori* region of interest (ROI) comprising the bilateral midbrain SN/VTA complex (manually delineated using the mean structural image from an independent sample of healthy participants^{27,79}), and the bilateral ventral (limbic) striatum (nucleus accumbens, ventral caudate rostral to the anterior commissure and ventral putamen rostral to the anterior commissure),⁸⁰ given these regions are implicated in model-free (habit) and model-based (goal directed) learning.^{7,10,14,15,25–27,63} We combined these two regions into a single ROI mask, defined in MNI space, to ensure that statistical results were corrected for the total number of voxels across both areas (see **SI Appendix Fig. S7** for an illustration of the ROI).

ROI activations were considered statistically significant at peak-level $P < 0.05$ family-wise error corrected using a small volume correction. For PET-fMRI correlations we extracted the principal eigenvariate of BOLD response from the relevant ROI sub-region (bilateral SN/VTA or ventral striatum). This measure reflects the 'typical' parameter estimate for a given contrast within a region, and is more robust to intra-regional heterogeneity of parameter estimates compared with the mean (using the mean parameter did not change the nature of the results). For whole brain analyses, we report BOLD activations that survive family-wise error correction at $P < 0.05$ at the cluster level (with cluster forming threshold set to $P < 0.001$ (unc.), to ensure a well behaved family error control).^{81,82}

PET analysis

We employed an automatic pipeline to obtain an individual parcellation of the brain into the studied regions of interest, implemented in MIAKAT release 4.2.6 (<http://www.miakat.org>),⁸³ SPM12 and FSL (version 5.0.9) (<https://fsl.fmrib.ox.ac.uk/fsl/fslwiki>). The simplified reference tissue model was used to derive the non-displaceable binding potential (BP_{ND}) of [¹¹C]-(+)-PHNO BP_{ND} from the regional time activity curves (**SI Appendix Eq. 11**),^{84,85} with cerebellar grey matter as the reference region. For each ROI we estimated baseline dopamine-2/3 receptor availability (BP_{ND}) and dexamphetamine-induced dopamine release (ΔBP_{ND} , the percentage reduction in BP_{ND} from the baseline to dexamphetamine scan, **SI Appendix Eq. 12**). See **SI Appendix** for further details.

Statistical analysis of PET-fMRI relationship

We tested for the hypothesised PET-fMRI correlations both using an *a priori* ROI analysis (SN/VTA and ventral striatum) and at the whole brain voxel level (see **SI Appendix** for further details). PET outcome measures were BP_{ND} and dexamphetamine-induced ΔBP_{ND} . The fMRI outcome measure was the contrast parameter estimate for Bayesian or information-theoretic surprise (voxel parameter estimate for whole brain analysis; principle eigenvariate of the parameter estimate for ROI analysis). For PET-fMRI ROI correlations we used Spearman's rank correlation coefficient, as we did not assume linear monotonic relationships (correlations remain significant when using Pearson's correlation coefficient).

ACKNOWLEDGEMENTS

We thank the MRI and PET technicians and radiographers at the Imanova Centre for Imaging Sciences, and Mark Ungless and Robert McCutcheon for comments on the initial manuscript. This study was funded by Medical Research Council-UK (no. MC-A656-5QD30), and Wellcome Trust (no. 094849/Z/10/Z) grants to O.H. and the National Institute for Health Research Biomedical Research Centre at South London and Maudsley NHS Foundation Trust and King's College London. M.N. is supported by the National institute for Health Research UK. T.D. is supported by an EU-FP7 MC6 ITN IN-SENS grant (grant number 607616). R.A. is supported by the Academy of Medical Sciences (AMS-SGCL13-Adams) and the National Institute of Health Research (CL-2013-18-003). R.D. is supported by a Wellcome Senior Investigator Award (098362/Z/12/Z). The Max Planck UCL Centre is a joint initiative supported by UCL and the Max Planck Society.

REFERENCES

1. Gershman, S. J., Norman, K. A. & Niv, Y. Discovering latent causes in reinforcement learning. *Curr. Opin. Behav. Sci.* **5**, 43–50 (2015).
2. Barto, A., Mirolli, M. & Baldassarre, G. Novelty or Surprise? *Front. Psychol.* **4**, 907 (2013).
3. Matsumoto, M. & Hikosaka, O. Two types of dopamine neuron distinctly convey positive and negative motivational signals. *Nature* **459**, 837–841 (2009).
4. Grace, A. A. Phasic versus tonic dopamine release and the modulation of dopamine system responsivity: A hypothesis for the etiology of schizophrenia. *Neuroscience* **41**, 1–24 (1991).
5. Lisman, J. E. & Grace, A. a. The hippocampal-VTA loop: Controlling the entry of information into long-term memory. *Neuron* **46**, 703–713 (2005).
6. Bunzeck, N. & Düz el, E. Absolute Coding of Stimulus Novelty in the Human Substantia Nigra/VTA. *Neuron* **51**, 369–379 (2006).
7. Schultz, W., Dayan, P. & Montague, P. R. A Neural Substrate of Prediction and Reward. *Science* **275**, 1593–1599 (1997).
8. Bromberg-Martin, E. S. & Hikosaka, O. Midbrain dopamine neurons signal preference for advance information about upcoming rewards. *Neuron* **63**, 119–126 (2009).
9. Daw, N. D., Gershman, S. J., Seymour, B., Dayan, P. & Dolan, R. J. Model-Based Influences on Humans Choices and Striatal Prediction Errors. *Neuron* **69**, 1204–1215 (2011).
10. Sharpe, M. J. *et al.* Dopamine transients are sufficient and necessary for acquisition of model-based associations. *Nat. Neurosci.* **20**, 735–742 (2017).
11. Gershman, S. J. The successor representation: its computational logic and neural substrates. *J. Neurosci.* 0151-18 (2018). doi:10.1523/JNEUROSCI.0151-18.2018
12. Starkweather, C. K., Gershman, S. J. & Uchida, N. The Medial Prefrontal Cortex Shapes Dopamine Reward Prediction Errors under State Uncertainty. *Neuron* **98**, 1–14 (2018).
13. Babayan, B. M., Uchida, N. & Gershman, S. J. Belief state representation in the dopamine system. *Nat. Commun.* **9**, (2018).
14. Takahashi, Y. K. *et al.* Dopamine Neurons Respond to Errors in the Prediction of Sensory Features of Expected Rewards. *Neuron* **95**, 1395–1405 (2017).
15. Chang, C. Y., Gardner, M., Di Tillio, M. G. & Schoenbaum, G. Optogenetic Blockade of Dopamine Transients Prevents Learning Induced by Changes in Reward Features. *Curr. Biol.* **27**, 3480–3486 (2017).
16. Itti, L. & Baldi, P. Bayesian surprise attracts human attention. *Vision Res.* **49**, 1295–1306 (2009).
17. Maia, T. V. & Frank, M. J. An Integrative Perspective on the Role of Dopamine in Schizophrenia. *Biol. Psychiatry* **81**, 52–66 (2017).
18. Kapur, S. Psychosis as a State of Aberrant Salience: A Framework Linking Biology, Phenomenology and Pharmacology in Schizophrenia. *Am J Psychiatry* **160**, 13–23 (2003).
19. Howes, O. D. & Nour, M. M. Dopamine and the aberrant saience hypothesis of schizophrenia. *World Psychiatry* **15**, 3–4 (2016).
20. Grace, A. A. Dysregulation of the dopamine system in the pathophysiology of schizophrenia and depression. *Nat. Rev. Neurosci.* **17**, 524–532 (2016).
21. Roiser, J. P. *et al.* Do patients with schizophrenia exhibit aberrant salience? *Psychol. Med.* **39**, 199–209 (2009).
22. Roiser, J. P., Howes, O. D., Chaddock, C. A., Joyce, E. M. & McGuire, P. Neural and behavioral correlates of aberrant salience in individuals at risk for psychosis. *Schizophr. Bull.* **39**, 1328–1336 (2013).
23. Heinz, A. Dopaminergic dysfunction in alcoholism and schizophrenia--psychopathological and behavioral correlates. *Eur. Psychiatry* **17**, 9–16 (2002).
24. Belujon, P. & Grace, A. A. Regulation of dopamine system responsivity and its adaptive and pathological response to stress. *Proc. R. Soc. B Biol. Sci.* **282**, (2015).
25. Iglesias, S. *et al.* Hierarchical Prediction Errors in Midbrain and Basal Forebrain during Sensory

- Learning. *Neuron* **80**, 519–530 (2013).
26. Boorman, E. D., Rajendran, V. G., O'Reilly, J. X. & Behrens, T. E. Two Anatomically and Computationally Distinct Learning Signals Predict Changes to Stimulus-Outcome Associations in Hippocampus. *Neuron* **89**, 1343–1354 (2016).
 27. Schwartenbeck, P., FitzGerald, T. H. B. & Dolan, R. Neural signals encoding shifts in beliefs. *Neuroimage* **125**, 578–586 (2016).
 28. O'Reilly, J. X. *et al.* Dissociable effects of surprise and model update in parietal and anterior cingulate cortex. *Proc. Natl. Acad. Sci. U. S. A.* **110**, E3660-3669 (2013).
 29. Sokoloff, P. & Le Foll, B. The dopamine D3 receptor, a quarter century later. *Eur. J. Neurosci.* **45**, 2–19 (2017).
 30. Diaz, J. *et al.* Dopamine D3 receptors expressed by all mesencephalic dopamine neurons. *J. Neurosci.* **20**, 8677–8684 (2000).
 31. Levant, B. The D3 Dopamine Receptor: Neurobiology and Potential Clinical Relevance. *Pharmacol. Rev.* **49**, 231–252 (1997).
 32. Fleckenstein, A. E., Volz, T. J., Riddle, E. L., Gibb, J. W. & Hanson, G. R. New insights into the mechanism of action of amphetamines. *Annu. Rev. Pharmacol. Toxicol.* **47**, 681–698 (2007).
 33. Daberkow, D. P. *et al.* Amphetamine paradoxically augments exocytotic dopamine release and phasic dopamine signals. *J. Neurosci.* **33**, 452–63 (2013).
 34. Covey, D. P., Bunner, K. D., Schuweiler, D. R., Cheer, J. F. & Garris, P. A. Amphetamine elevates nucleus accumbens dopamine via an action potential-dependent mechanism that is modulated by endocannabinoids. *Eur. J. Neurosci.* **43**, 1661–1673 (2016).
 35. Paladini, C. A., Fiorillo, C. D., Morikawa, H. & Williams, J. T. Amphetamine selectively blocks inhibitory glutamate transmission in dopamine neurons. *Nat. Neurosci.* **4**, 275–281 (2001).
 36. Cools, R. & D'Esposito, M. Inverted-U-shaped dopamine actions on human working memory and cognitive control. *Biol. Psychiatry* **69**, e113–e125 (2011).
 37. Green, C. E. L. *et al.* Measuring ideas of persecution and social reference: the Green *et al.* Paranoid Thought Scales (GPTS). *Psychol. Med.* **38**, 101–111 (2008).
 38. Matuskey, D. *et al.* Age-related changes in binding of the D2/3 receptor radioligand [¹¹C](+)PHNO in healthy volunteers. *Neuroimage* **130**, 241–247 (2016).
 39. Caravaggio, F. *et al.* Ventral striatum binding of a dopamine D2/3 receptor agonist but not antagonist predicts normal body mass index. *Biol. Psychiatry* **77**, 196–202 (2015).
 40. Badre, D., Doll, B. B., Long, N. M. & Frank, M. J. Article Rostrolateral Prefrontal Cortex and Individual Differences in Uncertainty-Driven Exploration. *Neuron* **73**, 595–607 (2012).
 41. Marshall, L. *et al.* Pharmacological Fingerprints of Contextual Uncertainty. *PLOS Biol.* **14**, e1002575 (2016).
 42. Iglesias, S., Tomiello, S., Schneebeli, M. & Stephan, K. E. Models of neuromodulation for computational psychiatry. *Wiley Interdiscip. Rev. Cogn. Sci.* **8**, e1420 (2017).
 43. Tziortzi, A. C. *et al.* Imaging dopamine receptors in humans with [¹¹C](+)PHNO: Dissection of D3 signal and anatomy. *Neuroimage* **54**, 264–277 (2011).
 44. Searle, G. E. *et al.* Mathematical modelling of [¹¹C](+)PHNO human competition studies. *Neuroimage* **68**, 119–132 (2013).
 45. Caravaggio, F. *et al.* Estimating Endogenous Dopamine Levels at D2 and D3 Receptors in Humans using the Agonist Radiotracer [(11)C](+)PHNO. *Neuropsychopharmacology* **39**, 2769–76 (2014).
 46. Koeltzow, T. E. *et al.* Alterations in dopamine release but not dopamine autoreceptor function in dopamine D3 receptor mutant mice. *J. Neurosci.* **18**, 2231–2238 (1998).
 47. Zapata, A. & Shippenberg, T. S. D3 receptor ligands modulate extracellular dopamine clearance in the nucleus accumbens. *J. Neurochem.* **81**, 1035–1042 (2002).
 48. Murphy, A. *et al.* Acute D3 Antagonist GSK598809 Selectively Enhances Neural Response During Monetary Reward Anticipation in Drug and Alcohol Dependence. *Neuropsychopharmacology* **42**, 1925–1926 (2017).

49. Groman, S. M. *et al.* Dopamine D3 Receptor Availability Is Associated with Inflexible Decision Making. *J. Neurosci.* **36**, 6732–6741 (2016).
50. Ferenczi, E. A. *et al.* Prefrontal cortical regulation of brainwide circuit dynamics and reward-related behavior. *Science* **351**, aac9698 (2016).
51. Belujon, P., Jakobowski, N. L., Dollish, H. K. & Grace, A. A. Withdrawal from Acute Amphetamine Induces an Amygdala-Driven Attenuation of Dopamine Neuron Activity: Reversal by Ketamine. *Neuropsychopharmacology* **41**, 619–627 (2016).
52. Shi, W.-X., Pun, C. L., Smith, P. L. & Bunney, B. S. Endogenous dopamine-mediated feedback inhibition of dopamine neurons: involvement of both D(1)- and D(2)-like receptors. *Synapse* **35**, 111–119 (2000).
53. Lodge, D. J. & Grace, A. A. Amphetamine activation of hippocampal drive of mesolimbic dopamine neurons: A mechanism of behavioral sensitization. *J. Neurosci.* **28**, 7876–7882 (2008).
54. Shi, W. X., Pun, C. L., Zhang, X. X., Jones, M. D. & Bunney, B. S. Dual effects of D-amphetamine on dopamine neurons mediated by dopamine and nondopamine receptors. *J. Neurosci.* **20**, 3504–3511 (2000).
55. Stachenfeld, K. L., Botvinick, M. M. & Gershman, S. J. The hippocampus as a predictive map. *Nat. Neurosci.* **20**, 1643–1653 (2017).
56. Behrens, T. E. J. *et al.* What is a cognitive map? Organising knowledge for flexible behaviour. *bioRxiv* (2018). doi:<https://doi.org/10.1101/365593>
57. Mack, M. L., Love, B. C. & Preston, A. R. Dynamic updating of hippocampal object representations reflects new conceptual knowledge. *Proc. Natl. Acad. Sci.* **113**, 13203–13208 (2016).
58. Hunt, L. *et al.* Triple dissociation of attention and decision computations across prefrontal cortex. *Nat. Neurosci.* **21**, 1471–1481 (2018).
59. Katthagen, T. *et al.* Modeling subjective relevance in schizophrenia and its relation to aberrant salience. *PLoS Comput. Biol.* **14**, e1006319 (2018).
60. Behrens, T. E. J., Woolrich, M. W., Walton, M. E. & Rushworth, M. F. S. Learning the value of information in an uncertain world. *Nat. Neurosci.* **10**, 1214–1221 (2007).
61. Tomov, M. S., Dorfman, H. M. & Gershman, S. J. Neural Computations Underlying Causal Structure Learning. *J. Neurosci.* **38**, 3336–17 (2018).
62. Glascher, J., Daw, N., Dayan, P. & Doherty, J. P. O. States versus Rewards: Dissociable Neural Prediction Error Signals Underlying Model-Based and Model-Free Reinforcement Learning. *Neuron* **66**, 585–595 (2010).
63. Diederer, K. M. M. J., Spencer, T., Vestergaard, M. D. D., Fletcher, P. C. C. & Schultz, W. Adaptive Prediction Error Coding in the Human Midbrain and Striatum Facilitates Behavioral Adaptation and Learning Efficiency. *Neuron* **90**, 1127–1138 (2016).
64. O’Doherty, J. P., Dayan, P., Friston, K., Critchley, H. & Dolan, R. J. Temporal difference models and reward-related learning in the human brain. *Neuron* **38**, 329–337 (2003).
65. Schlagenhaut, F. *et al.* Ventral striatal prediction error signaling is associated with dopamine synthesis capacity and fluid intelligence. *Hum. Brain Mapp.* **34**, 1490–1499 (2013).
66. Deserno, L. *et al.* Ventral striatal dopamine reflects behavioral and neural signatures of model-based control during sequential decision making. *Proc Natl Acad Sci U S A* **112**, 1595–1600 (2015).
67. Ballard, I., Miller, E. M., Piantadosi, S. T., Goodman, N. D. & McClure, S. M. Beyond Reward Prediction Errors: Human Striatum Updates Rule Values During Learning. *Cereb. Cortex* 1–11 (2017). doi:10.1093/cercor/bhx259
68. Syed, E. C. J. *et al.* Action initiation shapes mesolimbic dopamine encoding of future rewards. *Nat. Neurosci.* **19**, 34–36 (2016).
69. Guitart-Masip, M. *et al.* Action dominates valence in anticipatory representations in the human striatum and dopaminergic midbrain. *J Neurosci* **31**, 7867–7875 (2011).

70. FitzGerald, T. H. B., Schwartenbeck, P. & Dolan, R. J. Reward-Related Activity in Ventral Striatum Is Action Contingent and Modulated by Behavioral Relevance. *J. Neurosci.* **34**, 1271–1279 (2014).
71. Howard, J. & Kahnt, T. Identity prediction errors in the human midbrain update reward-identity expectations in the orbitofrontal cortex. *Nat. Commun.* **9**, 1–8 (2018).
72. Adams, R. A., Stephan, K. E., Brown, H. R., Frith, C. D. & Friston, K. J. The computational anatomy of psychosis. *Front. psychiatry* **4**, 47 (2013).
73. Auerbach, E. J., Xu, J., Yacoub, E., Moeller, S. & Uğurbil, K. Multiband accelerated spin-echo echo planar imaging with reduced peak RF power using time-shifted RF pulses. *Magn. Reson. Med.* **69**, 1261–1267 (2013).
74. Cauley, S. F., Polimeni, J. R., Bhat, H., Wald, L. L. & Setsompop, K. Interslice leakage artifact reduction technique for simultaneous multislice acquisitions. *Magn. Reson. Med.* **72**, 93–102 (2014).
75. Setsompop, K. *et al.* Blipped-controlled aliasing in parallel imaging for simultaneous multislice echo planar imaging with reduced g-factor penalty. *Magn. Reson. Med.* **67**, 1210–1224 (2012).
76. Xu, J. *et al.* NeuroImage Evaluation of slice accelerations using multiband echo planar imaging at 3 T. *Neuroimage* **83**, 991–1001 (2013).
77. Narendran, R. *et al.* Dopamine (D2/3) Receptor Agonist Positron Emission Tomography Radiotracer [11C]-(+)-PHNO is a D3 Receptor Preferring Agonist In Vivo. *Synapse* **60**, 485–495 (2006).
78. Asghar, S. J., Tanay, V. A. M. I., Baker, G. B., Greenshaw, A. & Silverstone, P. H. Relationship of plasma amphetamine levels to physiological, subjective, cognitive and biochemical measures in healthy volunteers. *Hum. Psychopharmacol.* **18**, 291–299 (2003).
79. Schwartenbeck, P., FitzGerald, T. H. B., Mathys, C., Dolan, R. & Friston, K. The Dopaminergic Midbrain Encodes the Expected Certainty about Desired Outcomes. *Cereb. Cortex* **25**, 3434–3445 (2015).
80. Martinez, D. *et al.* Imaging Human Mesolimbic Dopamine Transmission With Positron Emission Tomography. Part II: Amphetamine-Induced Dopamine Release in the Functional Subdivisions of the Striatum. *J. Cereb. Blood Flow Metab.* **23**, 285–300 (2003).
81. Eklund, A., Nichols, T. E. & Knutsson, H. Cluster failure: Why fMRI inferences for spatial extent have inflated false-positive rates. *Proc. Natl. Acad. Sci.* **113**, 7900–7905 (2016).
82. Flandin, G. & Friston, K. J. Analysis of family-wise error rates in statistical parametric mapping using random field theory. *Hum. Brain Mapp.* **ePub ahead**, (2017).
83. Gunn, R. N., Coello, C. & Searle, G. Molecular Imaging And Kinetic Analysis Toolbox (MIAKAT)- A Quantitative Software Package for the Analysis of PET Neuroimaging Data. *J. Nucl. Med.* **57**, Supplement 2 1928 (2016).
84. Gunn, R. N., Lammertsma, A. A., Hume, S. P. & Cunningham, V. J. Parametric Imaging of Ligand-Receptor Binding in PET Using a Simplified Reference Region Model. *Neuroimage* **6**, 279–287 (1997).
85. Lammertsma, A. A. & Hume, S. P. Simplified reference tissue model for PET receptor studies. *Neuroimage* **4**, 153–158 (1996).

PNAS

www.pnas.org

Supplementary Information for

Dopaminergic basis for signaling belief updates, but not surprise, and the link to paranoia

Matthew M Nour, Tarik Dahoun, Philipp Schwartenbeck, Rick A Adams, Thomas HB FitzGerald, Christopher Coello, Matthew B Wall, Raymond J Dolan, Oliver D Howes

Corresponding Authors

Dr Matthew Nour, matthew.nour@kcl.ac.uk

PO63 Level 5, IOPPN, King's College London, 16 De Crespigny Park, London SE5 8AF

Professor Oliver Howes, oliver.howes@kcl.ac.uk

PO63 Level 5, IOPPN, King's College London, 16 De Crespigny Park, London SE5 8AF

This PDF file includes:

Supplementary Materials and Methods
Supplementary Results
Figures S1 to S7
Tables S1 to S6
References for SI Appendix

SUPPLEMENTARY MATERIALS AND METHODS

Subjects

The study was conducted at Imanova Centre for Imaging Sciences, London. 41 healthy volunteer subjects were initially recruited through local media and university advertisements. Subjects had no history of neuropsychiatric disorder, a negative urine drug screen prior to scanning, and provided written informed consent to take part in the experiment. Two subjects were excluded from fMRI analysis. One subject did not receive adequate training in the task prior to scanning owing to technical problems, and a second was unable to perform the task beyond chance level (correlation between subject performance and that of an 'ideal Bayesian observer' was $r = .04$, and this subject was the only one for whom this measure of performance was more than 3 standard deviations less than the group mean). Thirty-nine subjects were therefore included in the fMRI analysis.

Task Details

The task and training procedures were identical to a previously published study.¹ During training, subjects were familiarized with two visual and two auditory cues, and learned that for each sensory modality (visual and auditory) one cue could be considered 'good' (in that it predicted monetary gains with approx. 90% validity) and one was 'bad' (in that it predicted monetary losses with approx. 90% validity). Subjects were informed (correctly) that these identities would remain stable throughout the experiment. Training also familiarized subjects with the task structure (state transition probabilities and cue validity).

In the task itself, for any given trial subjects were simultaneously presented with one visual and one auditory cue, followed by a monetary outcome (gains or losses from 10-30p). They were informed that for any given trial only one cue modality (visual or auditory) was relevant for predicting the monetary outcome, and that the identity of the relevant (predictive) cue modality would remain stable for a short period of time, but would periodically switch (5-6 times) in a session of 60 trials. The goal of the task was to correctly track the identity of the relevant cue modality (i.e. the current task state) at each trial, using information from cue-outcome observations. At the end of each trial participants reported their belief regarding the current informative modality using an 11-point rating bar.

For each trial, cues were presented for 2 s, followed by a gap jittered between 2 and 8 s. The monetary outcome was then shown for 2 s. Subsequently, a rating bar appeared for 4 s, at which time subjects indicated their beliefs about the relevant (predictive) cue modality using an MRI-compatible button box, by moving a cursor on the rating bar from 1 (left extreme, indicating complete certainty that one cue modality was relevant) to 11 (right extreme, indicating complete certainty that the other cue modality was relevant). The identities of the left and right extremes of the rating bar were alternated for each session, and the cursor

was positioned randomly at either the left or right extreme of the rating bar at the appearance of the rating bar on each trial. The next trial started after an inter-trial interval (fixation cross) jittered between 1 and 3 s.

Subjects' ratings at the end of each trial were assumed to result from their belief about the relevant modality before seeing the monetary outcome (prior belief), and their estimation of the likelihood of the observed cue-outcome pairing under the two competing hypotheses about the identity of the task-relevant modality. Importantly, in half of the trials the visual and auditory cue had the same valence (i.e. both were 'good' or both were 'bad'). The monetary outcome of these trials was therefore not informative about the identity of the relevant cue modality. Crucially, however, 'noninformative' trials could still lead to an unexpected (surprising) observation in the (approximately 10% of) trials where the monetary outcome was improbable under both auditory and visual cues (leading to positive information-theoretic surprise, but zero Bayesian surprise). The remaining trials were 'informative', in that the visual and auditory cues predicted different outcomes. On these trials the observed monetary outcome would differentially favour one hypothesis about the relevant modality more than the other. Unexpected observations on these trials (i.e. monetary outcomes that were improbable under the participant's prior belief about the relevant modality) indicated a potential switch in the relevant modality. These observations were therefore associated with both positive information theoretic surprise and positive Bayesian surprise. Thus, the task de-correlated information-theoretic and Bayesian surprise. Mean winnings in the 39 subjects across 3 sessions of the fMRI task were £24.30 (SD £3.68).

Computational Modelling

To capture behaviour we used a simple Hidden Markov Model (HMM), identical to that used in a previous study using this task.¹

Here, across a session of length T trials, the system moves through hidden states $x_{1:T} \in \{1,2\}$ ('auditory cues relevant' corresponds to $x_t = 1$, 'visual cues relevant' corresponds to $x_t = 2$), which must be inferred from monetary outcomes $y_{1:T} \in \{1,2\}$ (wins correspond to $y_t = 1$, and losses to $y_t = 2$), auditory cues $a_{1:T} \in \{1,2\}$, and visual cues $v_{1:T} \in \{1,2\}$ (win-predicting 'good' cues correspond to $a_t = 1$ and $v_t = 1$, and loss-predicting 'bad' cues to $a_t = 2$ and $v_t = 2$), all of which are directly observed (t indicates the current trial). For clarity of notation, we additionally define $o_t = [y_t a_t v_t]$ as the specific combination of monetary outcome, auditory and visual cues observed on each trial. Transition probabilities between hidden states are encoded in a 2×2 matrix \mathbf{B} such that

$$\mathbf{B} = \begin{bmatrix} \delta & 1 - \delta \\ 1 - \delta & \delta \end{bmatrix} \quad \text{Eq. 1}$$

$$p(x_t = j | x_{t-1} = i) = b_{ij} \quad \text{Eq. 2}$$

where $1 - \delta$ specifies the probability of a switch (reversal) between states (i.e. a change in the identity of the relevant modality). Observation probabilities under each state were encoded in a 2 x 2 matrix \mathbf{A} where

$$\mathbf{A} = \begin{bmatrix} \psi & 1 - \psi \\ 1 - \psi & \psi \end{bmatrix} \quad \text{Eq. 3}$$

$$p(o_t = [i j k] | x_t = 1) = a_{ij} \quad \text{Eq. 4}$$

$$p(o_t = [i j k] | x_t = 2) = a_{ik} \quad \text{Eq. 5}$$

Here, the cue validity parameter ψ governs how reliably the relevant cue modality predicts the monetary outcome. Thus, good cues (of the relevant modality) predict a win with probability ψ , and a loss with probability $1 - \psi$, and bad cues the converse. Initial state probabilities $p(x_1)$ are assumed to be uniform.

Given the conditional independence properties of the HMM, trial-by-trial belief updating can be performed by iterative applications of Bayes rule:

$$p(x_t | o_{1:t}, \mathbf{A}, \mathbf{B}) = \frac{p(o_t | x_t, \mathbf{A}, \mathbf{B}) p(x_t | o_{1:t-1}, \mathbf{A}, \mathbf{B})}{p(o_t | o_{1:t-1}, \mathbf{A}, \mathbf{B})} \quad \text{Eq. 6}$$

, where for all trials $t > 1$, a subject's posterior belief about the task-relevant modality after observing the cue-outcome pair, $p(x_t | o_{1:t}, \mathbf{A}, \mathbf{B})$, is proportional to the product of their estimate of the likelihood of observing the cue-outcome pair under each hypothesis, $p(o_t | x_t, \mathbf{A}, \mathbf{B})$ (captured by the free parameter ψ) and their prior belief about the task-relevant modality, $p(x_t | o_{1:t-1}, \mathbf{A}, \mathbf{B})$. The prior belief is dependent on the posterior belief from the previous trial, $p(x_{t-1} | o_{1:t-1}, \mathbf{A}, \mathbf{B})$, and the participant's belief about the probability of states remaining stable from one trial to the next, $p(x_t | x_{t-1}, \mathbf{A}, \mathbf{B})$, captured by the free parameter δ .

$$p(x_t | o_{1:t-1}, \mathbf{A}, \mathbf{B}) = p(x_t | x_{t-1}, \mathbf{A}, \mathbf{B}) p(x_{t-1} | o_{1:t-1}, \mathbf{A}, \mathbf{B}). \quad \text{Eq. 7}$$

For brevity we ignore the dependence on model m , but this is implied.

We estimated the two free parameters (ψ and δ) using constrained maximum-likelihood estimation (both parameters constrained between 0.5 and 1.0, inclusive). To identify optimal parameter settings for each subject, the fitting algorithm (instantiated in the Matlab-routine *fmincon*) was specified to maximize the

explained variance (R^2) in a linear model in which observed behaviour (belief rating about relevant cue modality) was predicted by the Bayesian model's predicted belief about the relevant modality.

For our subsequent imaging analysis (both GLM1 and GLM2), we defined the following trial-by-trial regressors based on the fitted model for each subject:

$$\begin{aligned}\alpha_t &= D_{KL}(p(x_t|o_{1:t}, \mathbf{A}, \mathbf{B}) || p(x_t|o_{1:t-1}, \mathbf{A}, \mathbf{B})) & \text{Eq. 8} \\ &= \sum_{i=1}^2 (p(x_t = i|o_{1:t}, \mathbf{A}, \mathbf{B}) \ln \frac{p(x_t = i|o_{1:t}, \mathbf{A}, \mathbf{B})}{p(x_t = i|o_{1:t-1}, \mathbf{A}, \mathbf{B})})\end{aligned}$$

corresponding to the Bayesian surprise (D_{KL} from prior to posterior beliefs at each trial), and

$$\begin{aligned}\beta_t &= -\ln p(o_t|o_{1:t-1}, \mathbf{A}, \mathbf{B}) & \text{Eq. 9} \\ &= -\ln \sum_{i=1}^2 (p(o_t|x_t = i, \mathbf{A}, \mathbf{B})p(x_t = i|o_{1:t-1}, \mathbf{A}, \mathbf{B})),\end{aligned}$$

corresponding to the information-theoretic surprise (I_S) of an observation, given the prior belief. For GLM2 we also defined the entropy over prior beliefs at cue presentation ('model-derived uncertainty') as the following:

$$H_t = -\sum_{i=1}^2 (p(x_t = i|o_{1:t-1}, \mathbf{A}, \mathbf{B}) \ln p(x_t = i|o_{1:t-1}, \mathbf{A}, \mathbf{B})) \quad \text{Eq. 10}$$

MR Image Acquisition and Analysis

MR images were acquired using a Siemens MAGNETOM Verio 3-T MR scanner and a 32-channel phased-array head-coil. We acquired one high-resolution T1-weighted structural volume for the purpose of fMRI and PET coregistration, and B0 fieldmaps in order to unwarp EPI images during spatial pre-processing. The T1-weighted volume was acquired using a Magnetization Prepared Rapid Gradient Echo (MPRAGE) sequence using parameters from the Alzheimer's Disease Research Network (ADNI-GO; 160 slices x 240 x 256, TR = 2300 ms, TE = 2.98 ms, flip angle = 9°, 1 mm isotropic voxels, bandwidth = 240Hz/pixel, parallel imaging (PI) factor = 2).² B0 fieldmaps were acquired using a dual-echo gradient-echo sequence (TR = 599 ms, TE 1 = 5.19 ms, TE 2 = 7.65 ms, flip angle = 60°, 3 mm isotropic voxels, 55 axial slices, bandwidth = 260 Hz/pixel).

Each scanning session started with a 'sound test' to ensure that subjects could distinguish the task auditory cues confidently against background scanner noise. Foam head-restraint pads were used to minimize head

movement. Respiratory and cardiac activities were measured using a respiration band and finger pulse oximeter to allow for physiological noise correction in the imaging analysis.³

During pre-processing, fMRI time series were realigned to the mean image and unwarped using the B0 fieldmaps generated by the Fieldmap toolbox.⁴ Image normalization to MNI space was accomplished using the DARTEL toolbox,⁵ with 6mm full-width at half-maximum (FWHM) Gaussian kernel smoothing.

For the first level general linear model (GLM) described in the main text, we used model-derived participant-specific estimates for Bayesian surprise and information-theoretic surprise as the trial-by-trial regressors of interest at outcome presentation. This means that we can have a high degree of confidence that the resulting fMRI findings are closely related to individual participant belief updating behaviour. The pairwise correlations between the parametric regressors at outcome presentation are shown in **SI Appendix Table S6** and are numerically similar to those reported in a previous study using the same model.¹ As nuisance regressors, first level GLMs included 6 realignment parameters and 18 physiological noise parameters, derived via RETROICOR using Fourier expansions for the estimated phases of cardiac pulsation, respiration and cardio-respiratory interactions (3rd, 4th and 1st order, respectively),⁶⁻⁸ implemented in the PhysIO toolbox (<https://www.tnu.ethz.ch/en/home.html>³). Temporal derivatives were included to account for slice-timing effects. An AR(1) model was used to account for serial autocorrelations, and we applied a 128s high-pass filter.

In addition to the GLM used in the main analysis (referred to as GLM1, and outlined in the main text), we conducted a second analysis (GLM2) in which the 'subjective uncertainty' parametric regressor at cue onset was replaced with an estimate of entropy over prior beliefs derived from the participant-specific fitted model ('model-derived uncertainty', H , **SI Appendix Eq. 10**). The correlation between subjective uncertainty (in GLM1) and model-derived uncertainty (in GLM2) across all subjects was $r = .46$ [.39, .52]. Results from GLM2 are only reported for the analysis of belief uncertainty at cue onset (in comparison with GLM1), however all GLM2 results for neural encoding of Bayesian and information-theoretic surprise, and the significant PET-fMRI correlations, are quantitatively similar to those from GLM1. One additional participant was excluded from the GLM2 analysis, as the behavioural responses of this participant resulted in a rank deficient design matrix ($\delta = 0.5$ in participant number 23, resulting in a uniform H).

fMRI activation maps are displayed as overlays on the SPM default 152-subject T1-weighted average volume. Projections onto the inflated cortical surface are created using bspmview (<http://www.bobspunt.com/bspmview/>).

PET Image Acquisition and Analysis

Prior to injection of the radiotracer and starting the PET acquisition, each subject first received a low-dose computed tomography scan for attenuation and model-based scatter correction. Dynamic PET images were reconstructed using a filtered back-projection algorithm into 31 frames (8 x 15 seconds, 3 x 60 seconds, 5 x 120 seconds, 15 x 300 seconds) with a 128 matrix, a zoom of 2.6 and a transaxial Gaussian filter of 5mm.

Structural MR images were segmented using SPM functions to obtain grey matter masks used for the definition of the reference region during the kinetic analysis. The ICBM152 template was non-linearly warped to each subject's structural MRI, and the derived deformation parameters were applied to our neuroanatomical atlas, to obtain a parcellation of each subject's brain into the studied ROIs (bilateral whole striatum⁹ and SN/VTA^{1,10}). The MRI, associated individual parcellation and associated grey matter masks were then downsampled to the PET resolution (2mm). Dynamic PET images were corrected for motion using a frame-by-frame registration process with a mutual information cost function. For each subject the averaged PET image from the entire scan duration was registered to the downsampled structural MRI scan with rigid-body registration. The rigid body matrix was subsequently applied to the motion corrected dynamic PET. Regional time activity curves (TAC) were obtained by applying the downsampled individual anatomical parcellations to the motion corrected dynamic PET image.

The non-displaceable binding potential (BP_{ND}) of [¹¹C]-(+)-PHNO is defined as follows:

$$BP_{ND} = \frac{f_{ND} B_{max} (1 - \sigma)}{K_D} \quad \text{Eq. 11}$$

where f_{ND} the non-displaceable free fraction of PHNO in the brain, B_{max} is the total D2/3R density, σ is the fraction of receptors bound by endogenous dopamine, and $1/K_D$ is the affinity of radioligand for the target. The simplified reference tissue model (SRTM) was used to derive BP_{ND} from the regional TACs.^{11,12} We used cerebellar grey matter as the reference region, defined as the intersection of the warped cerebellum atlas¹³ and individual subject grey matter mask.

The magnitude of dexamphetamine-induced dopamine release for each subject was quantified as the percentage reduction in BP_{ND} in the dexamphetamine condition compared to the baseline (no dexamphetamine) condition.

$$\Delta BP_{ND} = 100 \cdot \frac{BP_{ND} (baseline) - BP_{ND} (dexamphetamine)}{BP_{ND} (baseline)} \% \quad \text{Eq. 12}$$

Statistical Analysis

Whole brain PET-fMRI analysis

In addition to ROI-level PET-fMRI correlations, we also investigated the PET-fMRI relationships of interest in a series of second level whole brain fMRI analyses. Specifically, we conducted two regression analysis on the estimated responses for Bayesian surprise from the first-level analysis. The first regression model included midbrain BP_{ND} as a regressor, and the second included whole striatum ΔBP_{ND} as a regressor. We then repeated this procedure on the estimated responses for information-theoretic surprise from the first-level analysis. In all four models we tested the negative linear relationship between fMRI and PET measures across all voxels showing group level significant activation for the original fMRI contrast (Bayesian or information-theoretic surprise) at whole brain cluster level. We used identical criteria for establishing statistical significance in these whole brain fMRI-PET analyses as in the fMRI activation analysis (i.e. $P < 0.05$, family-wise error corrected either at whole brain cluster level or using a small volume correction with the SN/VTA and ventral striatum ROI).

Behaviour-PET Statistical Analysis

Based on the existing literature we hypothesised that there would be an inverted-U relationship between the ability to flexibility update internal representations (measured as trial-by-trial behavioural sensitivity to meaningful information, i.e. the mean difference in reported belief update between informative and non-informative trials) and baseline D2/3R signalling in the striatum (indexed by the fraction of total D2/3Rs under tonic stimulation by endogenous dopamine, σ).¹⁴ Striatal [¹¹C]-(+)-PHNO BP_{ND} is sensitive to inter-individual differences in synaptic dopamine concentration,^{15,16} such that it is proportional not only to the total density of D2/3Rs (B_{max}), but also to the fraction of available D2/3Rs that are *not* bound by endogenous dopamine ($1 - \sigma$) (see **SI Appendix Eq. 11**).¹⁵ If cognitive flexibility shows an inverted-U relationship with the fraction of D2/3Rs tonically occupied by endogenous dopamine (σ), then it can be shown algebraically that cognitive flexibility will also show an inverted-U relationship with BP_{ND} .

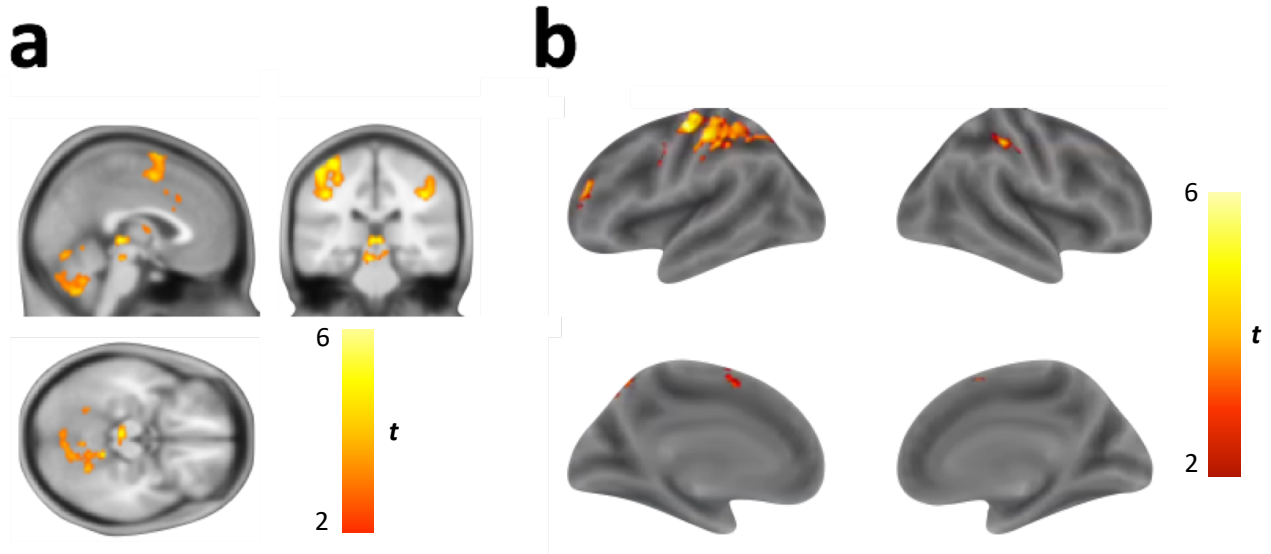
Throughout, we consider $P < 0.05$ as statistically significant. All statistical analyses were conducted using MATLAB Version 2015b.

SUPPLEMENTARY RESULTS

Behavioural Analysis

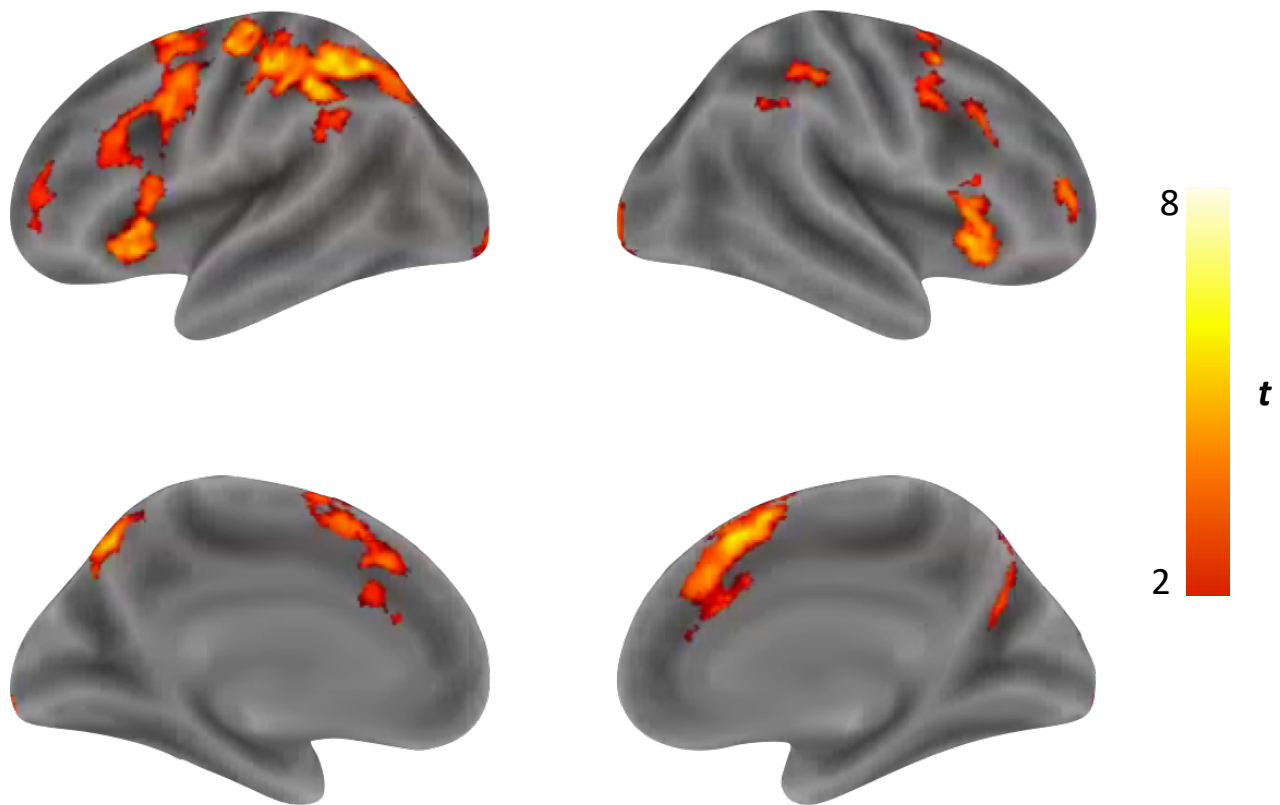
As outlined in the primary results, poor overall performance was positively correlated with the absolute magnitude of reported belief shifts on non-informative trials. This might reflect a tendency to increase belief uncertainty on non-informative trials (i.e. moving from one extremity of the rating bar, towards the middle indifference point, which may be adaptive), or a tendency to switch belief about the relevant modality from one hypothesis to a competing hypothesis (i.e. moving from one extremity of the rating bar to the other extremity, which is always maladaptive for non-informative trials). In support of the latter hypothesis, belief shifts on non-informative trials directly correlated with the mean number of times participants changed their belief about the relevant modality from one hypothesis to a competing hypothesis (termed a 'belief switch') on these trials ($\rho = .72$ [.52, .85], $P < 0.001$), but not with mean increase in reported belief uncertainty ($\rho = .21$ [-.12, .50], $P = 0.20$). Moreover, overall behavioural performance was negatively related to the mean number of belief switches in non-informative trials ($\rho = -.63$ [-.79, -.38], $P < 0.001$), but not informative trials ($\rho = -.19$ [-.49, .14], $P = 0.24$). In line with our findings that paranoia is related to maladaptive task performance, there was a positive correlation between paranoia and belief switches on non-informative trials ($\rho = .43$ [.13, .66], $P = 0.006$).

Fig. S1



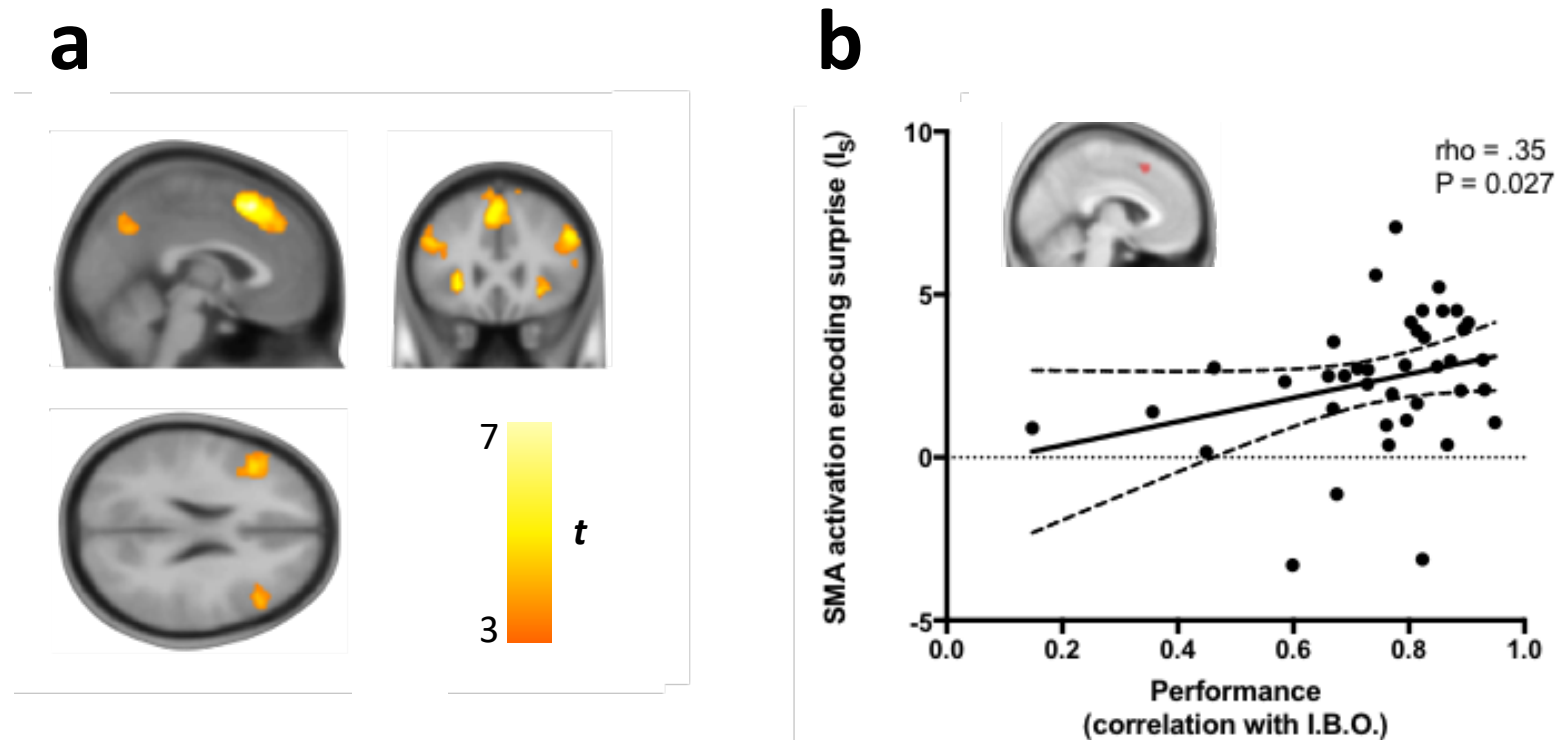
Brain regions showing significantly greater fMRI activation encoding Bayesian Surprise vs information theoretic Surprise ($D_{KL} > I_S$ t-contrast). (a): Small volume correction indicates that bilateral regions of the SN/VTA and ventral striatum encode D_{KL} to a significantly greater extent than they encode I_S . SN/VTA peaks: (Right peak Montreal Neurological Institute (MNI) coordinates, 12 -26 -12, $P_{peak} = 0.03$, $T_{peak} = 4.06$, and left peak MNI, -9 -26 -14, $P_{peak} = 0.03$, $T_{peak} = 4.03$). Ventral striatum peaks (left peak MNI, -12 -15 -4, $P_{peak} = 0.001$, $T_{peak} = 5.33$, and right peak MNI, 8 15 -4, $P_{peak} = 0.02$, $T_{peak} = 4.19$). Image thresholded at $P < 0.005$ (unc.) cluster extent threshold > 100 for illustration purposes only. (b): Significant clusters displayed at family-wise error corrected $P_{cluster} < 0.05$ (Voxel cut-off $P < 0.001$ (unc.), critical cluster threshold = 244), projected onto inflated cortical surface. Significant clusters include left middle frontal gyrus, left supplementary motor cortex, and bilateral parietal cortex. Colour bar represents t-values.

Fig S2



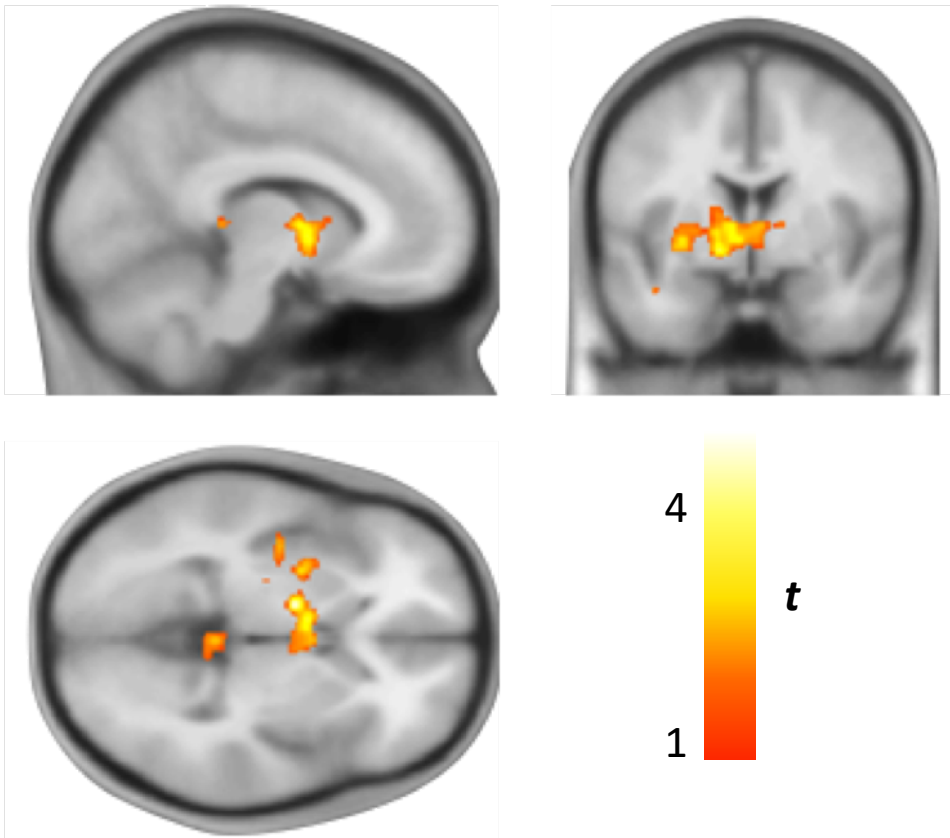
fMRI neural activity encoding Bayesian Surprise projected onto inflated cortical surface. Significant clusters of activation encoding Bayesian surprise across the whole brain displayed at family-wise error (FWE) corrected $P_{\text{cluster}} < 0.05$. (Voxel cut-off $P < 0.001$ (unc.), critical cluster threshold = 290), including posterior parietal cortex and lateral prefrontal cortex (see **SI Table S3** for details). Colour bar represents t-values.

Fig. S3



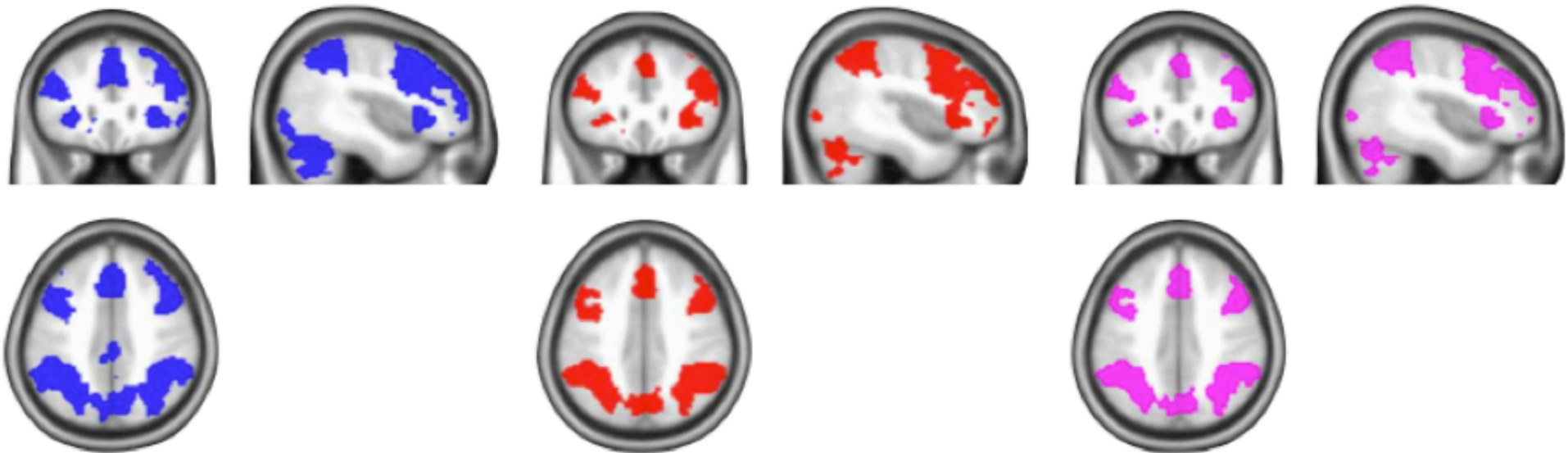
fMRI neural activity encoding information-theoretic surprise. (a) Clusters of activation encoding information-theoretic surprise across the whole brain, including the pre-supplementary motor area and left anterior insula. Image thresholded at $P < 0.001$ (unc.) with cluster extent threshold > 100 for illustration purposes only (see **SI Table S4** for family-wise error corrected cluster results). Colour bar represents t-values. (b) A cluster of voxels in the pre-supplementary motor area (shown in red) was significant at whole brain family-wise error (FWE) corrected $P_{\text{peak}} < 0.05$ level (peak Montreal Neurological Institute (MNI), -3 20 51, cluster size = 167, $P_{\text{peak}} = 0.001$, $T_{\text{peak}} = 7.72$). The effect size of this activation within this cluster (principle eigenvariate of parameter estimates for information-theoretic surprise contrast) positively correlated with participants' performance on the task (measured as the correlation between observed belief ratings and predictions of an ideal Bayesian observer (I.B.O.) model). Broken trendline represents 95% confidence bounds. SMA (pre-supplementary motor area).

Fig. S4



fMRI neural activity encoding signed reward prediction error. Clusters surviving whole brain family-wise error (FWE) correction at $P_{\text{cluster}} < 0.05$, applying a very liberal $P < 0.05$ (unc.) voxel-level cut-off. At this threshold there is a single large cluster of activation within the left striatum (peak Montreal Neurological Institute (MNI), -15 -3 -2, $P_{\text{cluster}} = 0.006$, $T_{\text{peak}} = 4.83$) surviving $P < 0.05$ corrected at whole brain level (critical cluster threshold = 4111). These results should be interpreted with caution given the very liberal cluster defining threshold used. Colour bar represents t-values.

Fig. S5



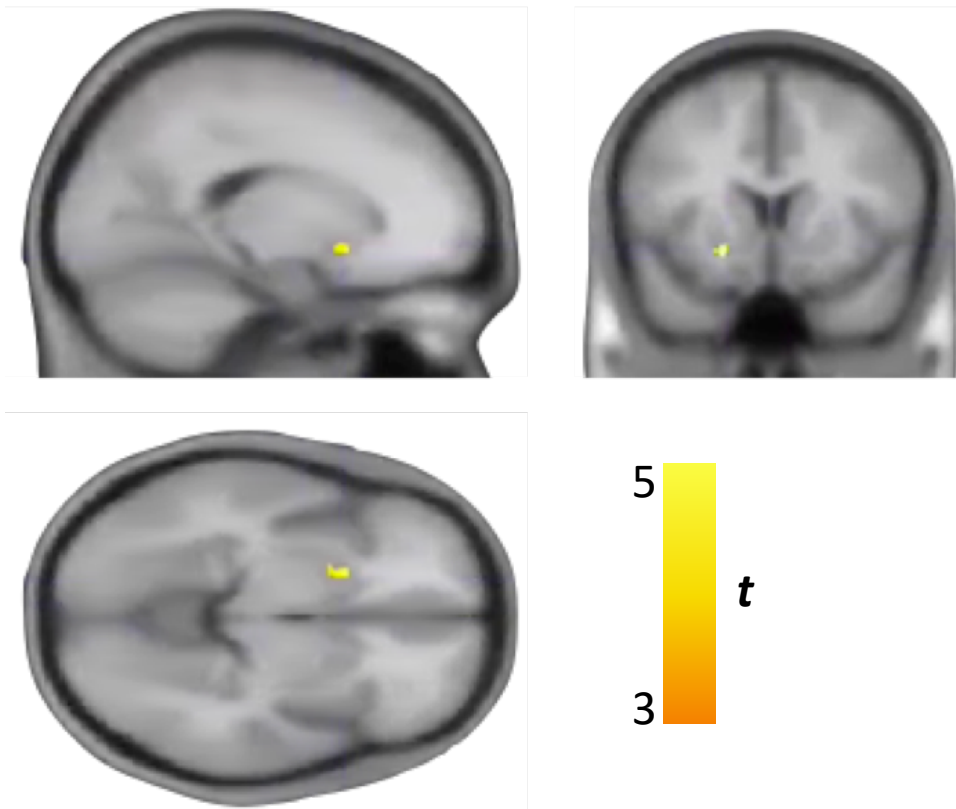
fMRI neural activity encoding uncertainty over prior beliefs at cue presentation.

Left: Subjective uncertainty: Blue clusters surviving whole brain family-wise error (FWE) correction at $P_{\text{cluster}} < 0.05$ from GLM1 (belief uncertainty at cue presentation defined as subjective uncertainty reported on rating bar on previous trial). See **SI Table S5** for details.

Middle: Model-derived uncertainty: Red clusters surviving whole brain FWE correction at $P_{\text{cluster}} < 0.05$ from GLM2 (belief uncertainty at cue presentation defined as entropy over model-derived prior belief distribution on the same trial). See **SI Table S5** for details.

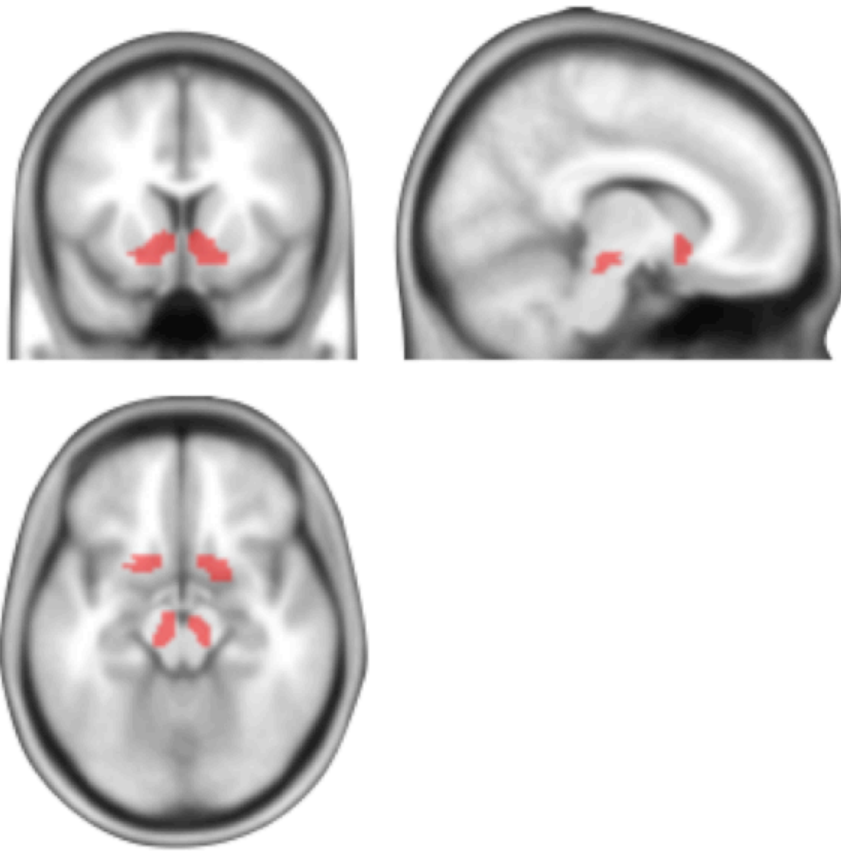
Right: Intersection: Violet clusters representing the intersection of voxels surviving whole brain FWE correction at $P_{\text{cluster}} < 0.05$ in both GLM1 and GLM2.

Fig. S6



Whole brain analysis showing voxels where a participant's neural activation (1st level parameter estimate) encoding Bayesian surprise is predicted by the participant's whole striatum dopamine release capacity, with a negative linear relationship. This relationship is significant following small volume correction (within combined SN/VTA and ventral striatum ROI) in the left ventral striatum (peak Montreal Neurological Institute (MNI) coordinates, -20 15 -9, $P_{\text{peak}} = 0.002$, $T_{\text{peak}} = 6.31$). Image thresholded at $P < 0.001$ (unc.) with inclusive ROI mask, for illustration purposes. Colour bar represents t-values.

Fig. S7



Combined substantia-nigra/ventral tegmental area (SN/VTA) and ventral striatum mask used for ROI analysis.
Masks derived from ^{1,9}.

Table S1

Mean individual parameter estimates of cue validity (ψ) and state transition probability ($1-\delta$).

| Participant | δ | ψ |
|--------------------|----------|--------|
| 1 | 0.83 | 0.96 |
| 2 | 0.98 | 0.95 |
| 3 | 0.94 | 0.76 |
| 4 | 0.93 | 0.81 |
| 5 | 0.94 | 0.86 |
| 6 | 0.97 | 0.97 |
| 7 | 0.91 | 0.98 |
| 8 | 0.97 | 0.98 |
| 9 | 0.93 | 0.93 |
| 10 | 0.97 | 0.89 |
| 11 | 0.97 | 0.99 |
| 12 | 0.90 | 0.76 |
| 13 | 0.96 | 0.97 |
| 14 | 0.91 | 0.71 |
| 15 | 0.96 | 0.96 |
| 16 | 0.92 | 0.89 |
| 17 | 0.99 | 0.93 |
| 18 | 0.94 | 0.88 |
| 19 | 0.94 | 0.96 |
| 20 | 0.95 | 0.96 |
| 21 | 0.82 | 0.96 |
| 22 | 0.93 | 0.97 |
| 23 | 0.50 | 0.89 |
| 24 | 0.95 | 0.91 |
| 25 | 0.89 | 0.90 |
| 26 | 0.88 | 0.65 |
| 27 | 0.90 | 0.63 |
| 28 | 0.91 | 0.84 |
| 29 | 0.85 | 0.95 |
| 30 | 0.93 | 0.93 |
| 31 | 0.95 | 0.83 |
| 32 | 0.83 | 1.00 |
| 33 | 0.93 | 0.83 |
| 34 | 0.97 | 0.94 |
| 35 | 0.97 | 0.99 |
| 36 | 0.98 | 0.84 |
| 37 | 0.91 | 1.00 |
| 38 | 0.89 | 0.97 |
| 39 | 0.93 | 0.95 |

Table S2

Results from the univariate (Model 1) and multivariate (Model 2) quadratic regression models, demonstrating an inverted-U relationship between striatal baseline D2/3R availability (BP_{ND}) and trial-by-trial behavioural sensitivity to meaningful information (mean belief shift on informative vs. non-informative trials). **Model 1:** *Behavioural sensitivity* = $\beta_0 + \beta_1 BP_{ND} + \beta_2 (BP_{ND})^2$, $F_{2,33} = 3.42$, adjusted $R^2 = .12$, model $P = 0.04$. **Model 2:** *Behavioural sensitivity* = $\beta_0 + \beta_1 BP_{ND} + \beta_2 Age + \beta_3 BMI + \beta_4 (BP_{ND})^2$, $F_{4,31} = 3.40$, adjusted $R^2 = .22$, model $P = 0.02$. Quadratic term has been mean-centred for both models. BMI = body mass index. BP_{ND} = [^{11}C]-(+)-PHNO non-displaceable binding potential within whole striatum region of interest.

| | β | Standard Error | T statistic | P value |
|----------------|---------|----------------|-------------|---------|
| Model 1 | | | | |
| Intercept | 0.89 | 0.94 | 0.95 | 0.35 |
| BP_{ND} | 0.50 | 0.44 | 1.13 | 0.26 |
| BP_{ND}^2 | -3.21 | 1.47 | -2.19 | 0.04 |
| | | | | |
| Model 2 | | | | |
| Intercept | 0.33 | 1.72 | 0.19 | 0.85 |
| BP_{ND} | 0.88 | 0.52 | 1.68 | 0.10 |
| Age | 0.04 | 0.02 | 1.81 | 0.08 |
| BMI | -0.05 | 0.03 | -1.70 | 0.10 |
| BP_{ND}^2 | -4.07 | 1.49 | -2.73 | 0.01 |

Table S3

Whole brain effects for Bayesian surprise (Kullback-Leibler divergence). Clusters of activation surviving whole brain family-wise error (FWE) corrected $P_{\text{cluster}} < 0.05$ threshold (voxel cut-off $P < 0.001$ (unc.), critical cluster threshold = 290). Anatomical label and MNI co-ordinates are reported for the voxel with the maximum t-statistic from each cluster. MNI (Montreal Neurological Institute), dACC (dorsal anterior cingulate cortex), pre-SMA (pre-supplementary motor area).

| Anatomical label | $P(\text{FWE})_{\text{cluster}}$ | Cluster size | T_{peak} | Z_{peak} | MNI coordinates (mm) | | |
|---|----------------------------------|--------------|-------------------|-------------------|----------------------|------|-----|
| | | | | | x | y | z |
| Left thalamus/brainstem | <0.001 | 1045 | 8.82 | 6.47 | -3 | -24 | 0 |
| Left pre-SMA/dACC (cluster includes left supramarginal gyrus and right middle/superior frontal gyrus) | <0.001 | 31924 | 7.64 | 5.91 | 0 | 9 | 60 |
| Left cerebellum | <0.001 | 1215 | 7.43 | 5.81 | -38 | -62 | -28 |
| Right cerebellum | <0.001 | 3450 | 6.3 | 5.18 | 36 | -51 | -32 |
| Right cerebellum | <0.001 | 1630 | 5.63 | 4.77 | 30 | -63 | -46 |
| Left occipital pole | 0.008 | 382 | 5.6 | 4.75 | -22 | -102 | -6 |
| Right middle frontal gyrus | 0.001 | 591 | 5.52 | 4.7 | 34 | 54 | 9 |
| Right occipital pole | 0.001 | 586 | 5.44 | 4.65 | 22 | -102 | -2 |
| Right precuneus / superior parietal lobule | 0.003 | 460 | 5.43 | 4.64 | 14 | -66 | 42 |
| Right supramarginal gyrus | 0.005 | 420 | 4.91 | 4.3 | 42 | -27 | 39 |
| Right angular gyrus / supramarginal gyrus | 0.029 | 290 | 4.91 | 4.29 | 48 | -46 | 42 |
| Left middle frontal gyrus | 0.001 | 578 | 4.86 | 4.26 | -33 | 45 | 8 |

Table S4

Whole brain effects for information-theoretic surprise. Clusters surviving whole brain family-wise error (FWE) corrected $P_{\text{cluster}} < 0.05$ threshold (voxel cut-off $P < 0.001$ (unc.), critical cluster threshold = 306). Anatomical label and MNI co-ordinates are reported for the voxel with the maximum t-statistic from each cluster. MNI (Montreal Neurological Institute), pre-SMA (pre-supplementary motor area).

| Anatomical label | $P(\text{FWE})_{\text{cluster}}$ | Cluster size | T_{peak} | Z_{peak} | MNI coordinates (mm) | | |
|---|----------------------------------|--------------|-------------------|-------------------|----------------------|-----|----|
| | | | | | x | y | z |
| Left pre-SMA | <0.001 | 3441 | 7.72 | 5.95 | -3 | 20 | 51 |
| Left anterior insula and inferior frontal gyrus | 0.016 | 310 | 5.92 | 4.95 | -28 | 24 | -3 |
| Right middle frontal gyrus and inferior frontal gyrus | <0.001 | 1582 | 5.83 | 4.9 | 50 | 22 | 30 |
| Left middle frontal gyrus | <0.001 | 1748 | 4.83 | 4.24 | -48 | 21 | 34 |
| Left angular gyrus and left superior parietal lobule | 0.017 | 306 | 4.67 | 4.12 | -32 | -63 | 42 |
| Precuneus (bilateral) | 0.002 | 451 | 4.3 | 3.85 | 3 | -64 | 34 |

Table S5

Whole brain effects for subjective belief uncertainty (GLM1) and model-derived belief uncertainty (entropy over prior beliefs) (GLM2) at cue onset. Clusters surviving whole brain family-wise error (FWE) corrected $P_{\text{cluster}} < 0.05$ threshold (voxel cut-off $P < 0.001$ (unc.), critical cluster threshold = 2343(GLM1) and 637(GLM2)). MNI co-ordinates are reported for the voxel with the maximum t-statistic from each cluster. MNI (Montreal Neurological Institute).

| Anatomical label | $P(\text{FWE})_{\text{cluster}}$ | Cluster size | T_{peak} | Z_{peak} | MNI coordinates (mm) | | |
|--|----------------------------------|--------------|-------------------|-------------------|----------------------|-----|-----|
| | | | | | x | y | z |
| GLM1 (subjective uncertainty) | | | | | | | |
| Bilateral frontal cortex (including dorsolateral prefrontal cortex and medial prefrontal cortex), anterior insula and subcortical structures (including striatum). | <0.001 | 49557 | 9.98 | 6.95 | -20 | 16 | 10 |
| Bilateral occipito-parietal cortex and cerebellum | <0.001 | 66515 | 9.57 | 6.79 | -38 | -72 | -50 |
| Middle and Posterior cingulate cortex | <0.001 | 2348 | 9.25 | 6.66 | -4 | -26 | 30 |
| GLM2 (model-derived uncertainty) | | | | | | | |
| Bilateral occipito-parietal cortex and cerebellum | <0.001 | 42790 | 8.95 | 6.49 | -10 | -80 | -34 |
| Right anterior insula and dorsolateral prefrontal cortex | <0.001 | 11433 | 7.23 | 5.67 | 33 | 30 | -3 |
| Left anterior insula and dorsolateral prefrontal cortex | <0.001 | 9043 | 7.12 | 5.61 | -27 | 24 | -3 |
| Medial prefrontal cortex (pre-supplementary motor area) | <0.001 | 2591 | 6.79 | 5.44 | 4 | 33 | 39 |
| Subcortical nuclei, including thalamus and striatum | <0.001 | 2210 | 6.3 | 5.16 | 9 | -6 | 9 |
| Left middle frontal gyrus | <0.001 | 1198 | 6.09 | 5.03 | -39 | 56 | 14 |
| Posterior cingulate cortex | <0.001 | 1030 | 5.33 | 4.56 | 3 | -36 | 27 |
| Right middle and inferior temporal gyrus | <0.001 | 1054 | 5.2 | 4.48 | 58 | -50 | -14 |
| Left middle and superior temporal gyrus | <0.001 | 637 | 4.43 | 3.94 | -64 | -40 | 3 |

Table S6

Mean pairwise correlations (Pearson's r) [and 95% C.I.] between parametric regressors at monetary outcome, used in the fMRI first-level general linear model (GLM).

| | Information-theoretic surprise | Reward prediction error | Money outcome |
|---------------------------------------|---------------------------------------|--------------------------------|----------------------|
| Bayesian-surprise | .53 [.49, .58] | -.002 [-.03, .02] | -.002 [-.02, .02] |
| Information-theoretic surprise | 1 | .019 [-.02, .05] | .008 [-.01, .02] |
| Reward prediction error | | 1 | .59 [.57, .61] |

REFERENCES FOR SI APPENDIX

1. Schwartenbeck P, FitzGerald THB, Dolan R. Neural signals encoding shifts in beliefs. *Neuroimage* 2016;125:578-586.
2. Jack CR, Bernstein MA, Fox NC, Thompson P, Alexander G, Harvey D, Borowski B, Britson PJ, Whitwell JL, Ward C, Dale AM, Felmlee JP, Gunter JL, Hill DLG, Killiany R, Schuff N, Fox-bosetti S, Lin C, Studholme C, Decarli CS, Krueger G, Ward HA, Metzger GJ, Scott KT, Mallozzi R, Blezek D, Levy J, Debbins JP, Fleisher AS, Albert M, Green R, Bartzokis G, Glover G, Mugler J, Weiner MW, Study A. The Alzheimer's Disease Neuroimaging Initiative (ADNI): MRI Methods. *J. Magn. Reson. Imaging* 2008;27(4):685-691.
3. Kasper L, Bollmann S, Diaconescu AO, Hutton C, Heinzle J, Iglesias S, Hauser T, Sebold M, Manjaly Z-M, Pruessmann K, Stephan K. The PhysIO Toolbox for Modelling Physiological Noise in fMRI Data. *J. Neurosci. Methods* 2017;276:56-72.
4. Hutton C, Bork A, Josephs O, Deichmann R, Ashburner J, Turner R. Image Distortion Correction in fMRI: A Quantitative Evaluation. *Neuroimage* 2002;16(1):217-240.
5. Ashburner J. A fast diffeomorphic image registration algorithm. *Neuroimage* 2007;38(1):95-113.
6. Glover GH, Li T, Ress D. Image-Based Method for Retrospective Correction of Physiological Motion Effects in fMRI: RETROICOR. *Magn. Reson. Med.* 2000;44:162-167.
7. Hutton C, Josephs O, Stadler J, Featherstone E, Reid A, Speck O, Bernarding J, Weiskopf N. The impact of physiological noise correction on fMRI at 7T. *Neuroimage* 2011;57(1-4):101-112.
8. Harvey AK, Pattinson KTS, Brooks JCW, Mayhew SD, Jenkinson M, Wise RG. Brainstem functional magnetic resonance imaging: Disentangling signal from physiological noise. *J. Magn. Reson. Imaging* 2008;28(6):1337-1344.
9. Martinez D, Slifstein M, Broft A, Mawlawi O, Hwang D-R, Huang Y, Cooper T, Kegeles L, Zarah E, Abi-Dargham A, Haber SN, Laruelle M. Imaging Human Mesolimbic Dopamine Transmission With Positron Emission Tomography. Part II: Amphetamine-Induced Dopamine Release in the Functional Subdivisions of the Striatum. *J. Cereb. Blood Flow Metab.* 2003;23(3):285-300.
10. Schwartenbeck P, FitzGerald THB, Mathys C, Dolan R, Friston K. The Dopaminergic Midbrain Encodes the Expected Certainty about Desired Outcomes. *Cereb. Cortex* 2015;25(10):3434-3445.
11. Gunn RN, Lammertsma AA, Hume SP, Cunningham VJ. Parametric Imaging of Ligand-Receptor Binding in PET Using a Simplified Reference Region Model. *Neuroimage* 1997;6(4):279-287.
12. Lammertsma AA, Hume SP. Simplified reference tissue model for PET receptor studies. *Neuroimage* 1996;4(3):153-158.
13. Tziortzi AC, Searle GE, Tzimopoulou S, Salinas C, Beaver JD, Jenkinson M, Laruelle M, Rabiner EA, Gunn RN. Imaging dopamine receptors in humans with [¹¹C]-(+)-PHNO: Dissection of D3 signal and anatomy. *Neuroimage* 2011;54(1):264-277.
14. Cools R, D'Esposito M. Inverted-U-shaped dopamine actions on human working memory and cognitive control. *Biol. Psychiatry* 2011;69(12):e113-e125.
15. Cox SML, Frank MJ, Larcher K, Fellows LK, Clark CA, Leyton M, Dagher A. NeuroImage Striatal D1 and D2 signaling differentially predict learning from positive and negative outcomes. *Neuroimage* 2015;109:95-101.
16. Caravaggio F, Nakajima S, Borlido C, Remington G, Gerretsen P, Wilson A, Houle S, Menon M, Mamo D, Graff-Guerrero A. Estimating Endogenous Dopamine Levels at D2 and D3 Receptors in Humans using the Agonist Radiotracer [¹¹C]-(+)-PHNO. *Neuropsychopharmacology* 2014;39(12):2769-76.